Mechanism and Machine Theory 167 (2022) 104558

Contents lists available at ScienceDirect

Mechanism and Machine Theory

journal homepage: www.elsevier.com/locate/mechmt

Research paper

# Compliance model of Exechon manipulators with an offset wrist

P.C. López-Custodio [a,*], R. Fu [d], J.S. Dai [b], Y. Jin [c]

[a] University of Lincoln, Brayford Way, LN6 7TS, Lincoln, Lincolnshire, UK
[b] King's College London, Strand, WC2R2LS, London, UK
[c] Queen's University Belfast, 123 Stranmillis Road BT9 5AH, Belfast, Northern Ireland, UK
[d] Dalian University of Technology, No. 2 Linggong Road, Ganjingzi District, Dalian City, Liaoning Province, PR China

ARTICLE INFO

*Keywords:*
Kinematics
Compliance
Parallel robots
Coupled kinematics
Stiffness

ABSTRACT

The stiffness of the Exechon hybrid manipulator is a crucial performance indicator as the manipulator is used as a 5-axis machine tool. Normally, the serial module of the Exechon is not included in the kinematic and stiffness analysis. In terms of kinematics, the parallel and serial modules are said to be decoupled, i.e. parallel module can be solved for position and the serial module can be used to compensate the parasitic orientation of the parallel platform. This is only possible when the serial module is a perfect spherical wrist. However, several models of Exechon technology have an offset wrist rather than a spherical one. Such an offset makes it impossible to obtain a kinematic decoupling.

In all publications available in the literature, the Exechon is considered to have a perfect spherical wrist. Therefore, this paper presents the inverse kinematics and compliance model of Exechon manipulators with offset wrists. The unknown coefficients in the compliance model are determined by optimizing the model against experimental data. The resulting predictions are then compared against more experimental results to validate the model.

## 1. Introduction

The use of parallel kinematic machines (PKM) or parallel manipulators [1,2] in industrial applications is relatively recent. Although a plethora of applications for the Delta robot and the Stewart platform [3,4] can be found in industry, most of the PKMs designs have not been exploited in production lines. An important reason for this is the relatively small workspace of conventional PKMs as well as their poor dexterity. Aiming to tackle this, the Tricept robot was presented [5,6] as a hybrid robot that combines a 3-DOF (degrees of freedom) parallel module with a 3-DOF serial module mounted in the parallel platform.

Simple in conception, the parallel module of the Tricept is basically a serial UP[1] chain which in turn is controlled by 3 actuated 6-DOF legs which do not add any constraints to the end-effector of the UP chain. Hence, the UP leg is fully unactuated making the control and manufacturing of the robot more complex. Vowing to get rid of this unactuated leg, the Exechon manipulator (see Fig. 1a) was designed as a new hybrid robot with an overconstrained 3-legged parallel module [7,8]. The Exechon has been already used in several applications, particularly, the Exechon is used in manufacturing [9] as a 5-axis machine.

Due to its application in manufacturing, the stiffness of the Exechon is important in order to improve the quality of the machined parts. Stiffness models for the parallel module of the Exechon are available in the literature [10–12] as they are for the Exechon-like 3-SPR machine developed in Tianjin University [13]. In general, researchers only focus in the parallel module of this hybrid machine due to its decoupled nature brought by the spherical wrist mounted as serial module. To the knowledge of the authors, all

* Corresponding author.
*E-mail addresses:* plopezcustodio@lincoln.ac.uk (P.C. López-Custodio), r.fu@dlut.edu.cn (R. Fu), jian.dai@kcl.ac.uk (J.S. Dai), y.jin@qub.ac.uk (Y. Jin).

[1] In this article: U stands for universal joint, P for prismatic joint, R for revolute joint and S for spherical joint.

https://doi.org/10.1016/j.mechmachtheory.2021.104558
Received 10 May 2021; Received in revised form 30 July 2021; Accepted 8 September 2021
Available online 4 October 2021

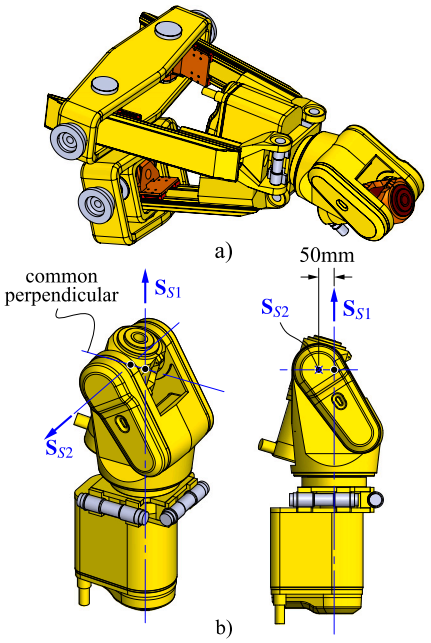


**Fig. 1.** (a) The Exechon XMini, (b) Offset in the wrist of the Exechon XMini.

the published papers that study the Exechon consider a perfectly spherical wrist. The spherical wrist allows the kinematic decoupling of the modules, using the parallel one for positioning and the serial one for orientating. The decoupling property is exploited when solving the kinematics of the Exechon [14–17] to obtain closed form solutions.

Nevertheless, among the fairly large number of Exechon models, there are some whose wrist is not spherical, but present an offset between the two axes of the R joints in the serial module. Fig. 1b shows the 2-DOF serial module of the Exechon XMini, Fig. 1a, a smaller model built of mainly carbon fiber. The two R joint axes of the wrist of the XMini will be called here $\mathbf{S}_{S1}$ and $\mathbf{S}_{S2}$. As shown in Fig. 1b, these axes do not intersect and an offset of 50 mm is present between them.

Although the complexity of obtaining a compliance model of the Exechon is indifferent to the type of wrist, the inverse kinematics, required to obtain the stiffness in each configuration, is severely affect and no closed form solution is expected for the problem, in a similar way to what happens with fully serial 6-DOF robots with offset wrists [18]. In its simplest form, without offset between joint axes, neither at the base, nor at the wrist, the inverse kinematics is not only decoupled, but also has closed form solution, see [14,16] where such a solution is presented.

In [17], we presented the position analyses of an Exechon robot featuring only the offsets at its base, but not at the wrist. The perfectly spherical wrist of the manipulator considered in such a publication still allowed the decoupling of position and orientation, however no closed form solution can be found. In this paper we first obtain the inverse kinematics of an Exechon manipulator, which not only features an offset writs, but it also presents offsets between the axes of the joints connecting the legs to the base.

Now in this paper, the addition of an offset at the wrist not only will allow the analysis of models like the XMini, whose nominal dimensions include such an offset, but it can also work as a completely generalized kinematic model in which such offsets can be seen as manufacturing errors and, thus, we can compute the total error at the end-effector due to such imperfections. Table 1 summarizes these three cases of Exechon manipulator.

In this paper, after the inverse kinematics of this Exechon manipulator with offset wrist is solved, a semi-analytical compliance model is obtained for the whole robot, considering both serial and parallel modules. See [19] for one of the few examples where the serial part of a hybrid robot, the Tricept, is considered in the stiffness model as a spherical wrist. See also [20] for an example of stiffness model of a hybrid (parallel–parallel) robot.

In general, if detailed information of the components that integrate the manipulator is known, an accurate compliance model can be built. However, it is common that many structural details of the machine are not known, including not only the materials the parts are made of, but also how the parts are mounted, the stiffness of the actuators after a complex transmission system is included, etc. Hence, in this paper we employ a different framework that allows modeling the compliance with less information of how the robot is built.

We first sketch a model based in the overall Jacobian matrix [13,19,21–25]. Other techniques for stiffness computation in parallel manipulators can be found in [26–30]. We then propose a quadratic in terms of the legs length to model the local compliance of a group of components modeled as a single element in the analysis. With this assumptions, the model can be written in terms of all the unknown quantities. Then, using experimental data, the model is optimized applying direct multi-search (DMS) [31] method. After

**Table 1**
Cases of offsets in the Exechon manipulator.

| | | | |
|---|---|---|---|
| | 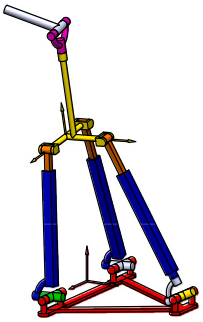 | 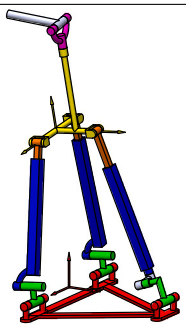 | 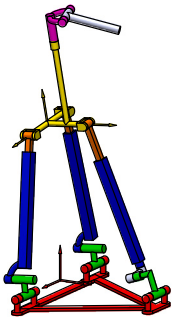 |
| Wrist | Spherical | Spherical | Offset |
| Base offsets | × | ✓ | ✓ |
| Decoupling | ✓ | ✓ | × |
| Closed form IK | ✓ | × | × |
| IK solved in | [14,16] | [17] | None |

the optimization, the unknown values in the model are determined and the model is able predict the compliance in any direction and in any configuration.

The rest of the paper is organized as follows: We first introduce the notation used throughout the paper in Section 2. Section 3 presents the geometry of the Exechon manipulator with offset wrist. Section 4 solves the coupled inverse kinematics of the robot. In Section 5, the system of constraints and that of actuations are obtained. The compliance equations are reminded in Section 6. In Section 7, the compliances of the different elements of the manipulator are computed in terms of several unknowns. Section 8 shows how these unknowns are obtained using an optimization process. In Section 9 these results are applied to a case study considering the Exechon XMini. Finally, in Section 10, some conclusions are drawn.

## 2. Notation

The notation used through the paper is now introduced.

The symbol ":=" is used for definition of variables. Three-dimensional vectors are written in lowercase bold letters, such as $\mathbf{v} \in \mathbb{R}^3$. $\mathbf{S} \in \mathbb{R}^6 \cong \mathrm{se}(3)$ is used for screw coordinate vectors. In order to avoid the introduction of more symbols, we use $\mathbf{S}$ for both the screw coordinates of an axis and the geometric element itself. Unit vectors are hatted, $\hat{\mathbf{u}} \in \mathbb{S}^2$. Dot product is represented by central dot $\cdot$, while matrix multiplication is denoted by juxtaposition, unless otherwise specified — see Section Section 7.

Coordinate systems are named with non-italic capital letters, while points are presented in italic capital letters. For example, in Fig. 2 frame O has origin at point $O$. Let A and B be two coordinate systems with origins at $A$ and $B$, respectively, and let $P$ and $Q$ be two points. Then the notation from [32] is used to manage coordinate systems. Namely, ${}^{\mathrm{A}}\mathbf{r}_{P/Q}$ is the vector from point $Q$ to point $P$ in coordinate system A. While ${}^{\mathrm{A}}\mathbf{r}_P := {}^{\mathrm{A}}\mathbf{r}_{P/A}$ is the position vector of point $P$ in frame A. ${}^{\mathrm{A}}_{\mathrm{B}}\mathbf{R} \in \mathrm{SO}(3)$ is the rotation matrix that relates the orientation of frame B to that of frame A, such that ${}^{\mathrm{A}}\mathbf{r}_P = {}^{\mathrm{A}}_{\mathrm{B}}\mathbf{R}\,{}^{\mathrm{B}}\mathbf{r}_P + {}^{\mathrm{A}}\mathbf{r}_B$. The canonical triad defining frame A but expressed in frame B is denoted by $\{{}^{\mathrm{B}}\hat{\mathbf{i}}_{\mathrm{A}}, {}^{\mathrm{B}}\hat{\mathbf{j}}_{\mathrm{A}}, {}^{\mathrm{B}}\hat{\mathbf{k}}_{\mathrm{A}}\}$

$d(P,Q) \in \mathbb{R}$ is the Euclidean distance between points $P$ and $Q$. $\mathrm{Rot}(\beta, \hat{\mathbf{v}}) \in \mathrm{SO}(3)$ is the rotation matrix representing a rotation of $\beta$ radians about an axis that passes through the origin and that is parallel to $\hat{\mathbf{v}}$. $\mathrm{Adj}(\psi) \in \mathbb{R}^{4\times4}$ returns the adjoint representation of Euclidean displacement $\psi \in \mathrm{SE}(3)$. Null() represents the null space of a matrix, while $()^{\mathrm{t}}$ is its transpose. Finally, aug() and diag() represent, respectively, the augmented matrix of an ordered set of column vectors, and the diagonal matrix with diagonal elements equal to an ordered set of scalars.

Table 2 gives a quick reference to important symbols used in the thesis.

## 3. Geometry of the Exechon manipulator

Fig. 2 shows a representation of an Exechon hybrid robot. The robot integrates a 3-DOF parallel module and a 2-DOF serial module. The parallel module consists of a moving platform and a fixed platform connected by three legs. Legs 1 and 3 are RRPR serial chains, while leg 2 is an RRRPR kinematic chain. From Fig. 2, if $i = 1, 3$, the following geometric constraints hold:

$\mathbf{S}_{i2} \| \mathbf{S}_{l4} \| \hat{\mathbf{n}}_{\Pi}$

$\mathbf{S}_{i1} \perp \hat{\mathbf{n}}_{\Pi}$, $\mathbf{S}_{i3} \perp \hat{\mathbf{n}}_{\Pi}$

$\mathbf{S}_{21} \perp \mathbf{S}_{22}$, $\mathbf{S}_{22} \perp \mathbf{S}_{23}$

$\mathbf{S}_{23} \parallel \mathbf{S}_{24}$, $\mathbf{S}_{24} \perp \mathbf{S}_{25}$

$\mathbf{S}_{25}$ and $\mathbf{S}_{i4}$ intersect perpendicularly

**Table 2**
Quick reference to some specific symbols.

| Symbol | Definition |
|---|---|
| $\mathbf{S}_{ij}$ | Screw axis of the $ij$ joint |
| $\hat{\mathbf{t}}$ | Unit vector parallel to the tool axis |
| $\hat{\mathbf{n}}_{\Pi}$ | Unit vector perpendicular to plane $\Pi$, see Fig. 2 |
| $\mathbf{W}_{cij}$, $\mathbf{W}_{ai}$ | Screw axes of wrench of constraint $cij$ and wrench of actuations $ai$ |
| $\mathbf{J}_{Pa}$, $\mathbf{J}_{Pc}$, $\mathbf{J}_{P}$ | Jacobian matrices of actuations, constraints and overall for the parallel module, respectively |
| $\mathbf{J}_{Sa}$, $\mathbf{J}_{Sc}$, $\mathbf{J}_{S}$ | Jacobian matrices of actuations, constraints and overall for the serial module, respectively |
| $\mathbf{C}_{P}$, $\mathbf{C}_{S}$ | Compliance matrices for the parallel and serial module, respectively |
| $\overline{\mathbf{C}}_{P}$, $\overline{\mathbf{C}}_{S}$ | Local compliance matrices for the parallel and serial module, respectively |
| $\mathbf{C}_{\Lambda,e}$, $\mathbf{C}_{\Theta,e}$ | Linear and torsional compliance matrices of element e |

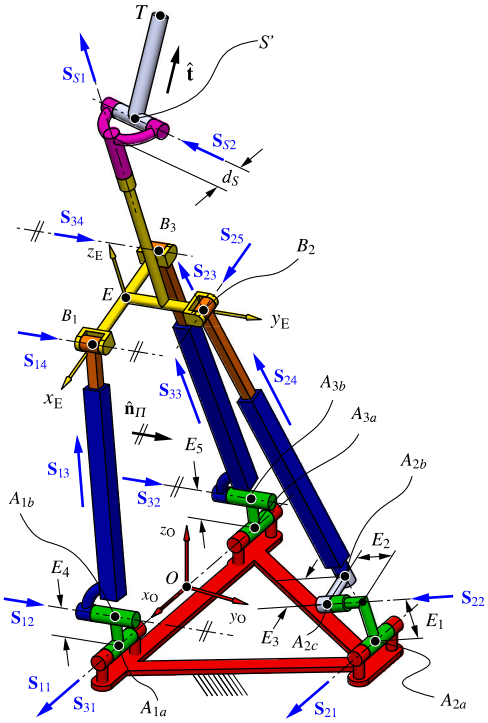


**Fig. 2.** Geometry of an Exechon manipulator with offset wrist.

Points $A_{1a}$, $A_{2a}$ and $A_{3a}$ are the vertices of an isosceles triangle with base $2d_{A1} := d(A_{1a}, A_{3a})$ and height $d_{A2} := d(A_{2a}, \mathbf{S}_{11})$. Points $B_1$, $B_2$ and $B_3$ also form an isosceles triangle with base $2d_{B1} := d(B_1, B_3)$ and height $d_{B2} := d(B_2, \overline{B_1 B_2})$.

For $i = 1, 3$, points $A_{ia}$, $A_{ib}$, and $B_i$ are coplanar, we call the plane that these point lie on $\Pi$, while plane $\Lambda$ is the one containing $B_1$, $B_2$ and $B_3$. The joint variables of the actuated joints of each leg are measured as follows: $q_{i3} := d(A_{ib}, B_i)$, $i = 1, 3$, and $q_{24} := d(A_{2b}, B_2)$.

The following offsets are considered between the joints connecting the legs to the base:

$$E_1 := d(\mathbf{S}_{21}, \mathbf{S}_{22}),\ E_2 := \hat{\mathbf{s}}_{22} \cdot \mathbf{r}_{A_{2b}/A_{2a}},$$
$$E_3 := d(\mathbf{S}_{22}, \mathbf{S}_{23}) = d(A_{2b}, A_{2c}),$$
$$E_4 := d(\mathbf{S}_{11}, \mathbf{S}_{12}),\ E_5 := d(\mathbf{S}_{31}, \mathbf{S}_{32})$$

The serial module is mounted on the moving platform. This module is a serial 2R chain with its two axes $\mathbf{S}_{S1}$ and $\mathbf{S}_{S2}$ being skew with a normal distance between them equal to $d_S$. These two revolute joints are used to orientate the spindle axis, which is parallel to $\hat{\mathbf{t}}$. Point $T$ represents the tool tip. Point $S'$ is the intersection of $\mathbf{S}_{S2}$ and the common perpendicular between $\mathbf{S}_{S1}$ and $\mathbf{S}_{S2}$. Therefore, the spindle axis is defined as $\mathscr{L}_T := \mathscr{L}(\hat{\mathbf{t}}, S')$. $S'$ is located a distance $h_z := d(S, \Lambda)$ from plane $\Lambda$, while $h_x := d(\mathbf{S}_{S1}, \Pi)$.

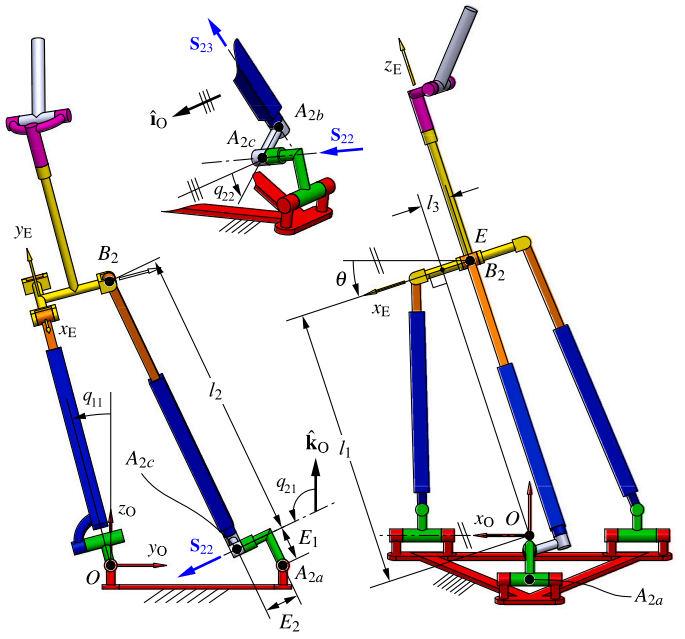


**Fig. 3.** Lateral views of the Exechon robot showing internal variables.

Axis $\mathbf{S}_{S1}$ is perpendicular to $\Lambda$ and the two axes constituting the serial module are perpendicular to each other. We define the tool length as $d_T := d(T, S')$.

In the nominal dimensions of all commercial Exechon robots, $E_i = 0, \forall i = 1, \dots, 5$. In all the analyses that can be found in the literature, $d_S$ is equal to 0, which allows a kinematic decoupling. However, as shown in Fig. 1, $d_S = 50$mm in the Exechon XMini.

We define three coordinate systems, O, E and F. Coordinate system O, $\{x_O, y_O, z_O\}$, has origin at $O$ and is attached to the fixed platform and is used as a global, fixed frame. $x_O$ and $y_O$ are coaxial with $\mathbf{S}_{11}$ and $\overline{OA_{2a}}$, respectively. Frame E, $\{x_E, y_E, z_E\}$ is attached to the moving platform and has origin at point $E$, the middle point of segment $\overline{B_1B_3}$. $x_E$ and $y_E$ are coaxial with $\overline{EB_1}$ and $\overline{EB_2}$, respectively. Note that $\hat{\mathbf{k}}_E \parallel \hat{\mathbf{n}}_{\Pi}$. Finally, coordinate system F has origin at $O$ and is parallel to frame E.

## 4. Inverse kinematics

The following information is known in the inverse kinematic problem (IKP): ${}^O\mathbf{r}_T$, i.e. the position of the tip of the tool, point $T$, with respect to the fixed coordinate system, and ${}^O\hat{\mathbf{t}} := (t_1, t_2, t_3) \in \mathbb{S}^2$, a unit vector that is parallel to the tool. The goal of the IKP is to determine the screw coordinates of all joint axes in the robot with respect to the fixed coordinate system: ${}^O\mathbf{S}_{1i}$, ${}^O\mathbf{S}_{3i}$, ${}^O\mathbf{S}_{2j}$ and ${}^O\mathbf{S}_{Sk}$, $i = 1, \dots, 4$, $j = 1, \dots, 5$, $k = 1, 2, 3$.

For this analysis, it is important to define the way the following joint variables are measured:

- $q_{11}$, from $\hat{\mathbf{j}}_O$ to $\hat{\mathbf{n}}_{\Pi}$ about $\mathbf{S}_{11}$.
- $q_{21}$, from $\hat{\mathbf{k}}_O$ to $\hat{\mathbf{s}}_{22}$ about $\mathbf{S}_{21}$.
- $q_{22}$, from $\hat{\mathbf{i}}_O$ to $\hat{\mathbf{s}}_{23} \times \hat{\mathbf{s}}_{22}$ about $\mathbf{S}_{22}$.
- $q_{S1}$, from $\hat{\mathbf{i}}_E$ to $\hat{\mathbf{s}}_{S2}$ about $\mathbf{S}_{S1}$.
- $q_{S2}$, from $\hat{\mathbf{k}}_E$ to $\hat{\mathbf{t}}$ about $\mathbf{S}_{S2}$.

We also define the following internal variables (see Fig. 3):

- $l_1$. The (shortest) distance between point $O$ and the $x_E$ axis, $l_1 = d(O, \overline{B_1, B_3}) = \mathbf{r}_{E/O} \cdot \hat{\mathbf{k}}_E$.
- $l_3$. The length of the projection of $\mathbf{r}_{E/O}$ on the $x_E$ axis, $l_3 = \mathbf{r}_{E/O} \cdot \hat{\mathbf{i}}_E$.
- $l_2$. The length of the projection of $\mathbf{r}_{B_2/A_{2c}}$ onto the $y_O z_O$ plane.
- $\theta$. The angle measured from $x_O$ to $x_E$ about $y_E$.

Using these variables it can be seen that ${}^O_E\mathbf{R} = {}^O_F\mathbf{R} = \text{Rot}(q_{11}, {}^O\hat{\mathbf{i}}_O)\text{Rot}(\theta, {}^O\hat{\mathbf{j}}_O)$. For the analysis we also use point $S'$, instead of $T$. The position of $S'$ is known from the input information of the IKP as $(x_{S'}, y_{S'}, z_{S'}) := {}^O\mathbf{r}_{S'/O} = {}^O\mathbf{r}_T - d_T{}^O\hat{\mathbf{t}}$.

The following constraints are considered in order to solve the IKP:

1. $\mathbf{S}_{23} \perp {}^{\mathrm{O}}\hat{\mathbf{i}}_{\mathrm{E}}$. Using revolute joints 21 and 22 to orientate $\mathbf{S}_{23}$, it follows ${}^{\mathrm{O}}\hat{\mathbf{s}}_{23} = \mathrm{Rot}(q_{21}, {}^{\mathrm{O}}\hat{\mathbf{i}}_{\mathrm{O}})\mathrm{Rot}(q_{22}, {}^{\mathrm{O}}\hat{\mathbf{k}}_{\mathrm{O}})^{\mathrm{O}}\hat{\mathbf{j}}_{\mathrm{O}}$. It is also known that ${}^{\mathrm{O}}\hat{\mathbf{i}}_{\mathrm{E}} = {}^{\mathrm{O}}_{\mathrm{E}}\mathbf{R}^{\mathrm{O}}\hat{\mathbf{i}}_{\mathrm{O}}$. This condition is thus expressed in terms of $\theta$, $q_{11}$, $q_{21}$ and $q_{22}$ as:

$$ {}^{\mathrm{O}}\hat{\mathbf{s}}_{23} \cdot {}^{\mathrm{O}}\hat{\mathbf{i}}_{\mathrm{E}} = 0 \tag{1} $$

2. The coordinates of $S'$ in frame F are easily obtained as $(-l_3 + d_S\cos(q_{S1} - \pi/2), h_y + d_S\sin(q_{S1} - \pi/2), l_1 + h_z)$. Therefore, this condition can be expressed in terms of $\theta$, $q_{11}$, $l_1$, $l_3$ and $q_{S1}$ by:

$$ {}^{\mathrm{F}}_{\mathrm{O}}\mathbf{R}^{\mathrm{O}}\mathbf{r}_{S'/O} = \begin{pmatrix} -l_3 + d_S\cos(q_{S1} - \pi/2) \\ h_y + d_S\sin(q_{S1} - \pi/2) \\ l_1 + h_z \end{pmatrix} \tag{2} $$

3. The $y_{\mathrm{O}}$ coordinate of point $B_2$ can be recognized as $d_{A2} + (l_2 + E_1)\cos(q_{21}) - E_2\sin q_{21}$. It is also known that ${}^{\mathrm{F}}\mathbf{r}_{B_2} = (-l_3, d_{B_2}, l_1)$, therefore, this condition can be expressed in terms of $q_{11}$, $\theta$, $q_{21}$, $l_3$ and $l_2$ by:

$$ {}^{\mathrm{O}}_{\mathrm{F}}\mathbf{R}^{\mathrm{F}}\mathbf{r}_{B_2} \cdot {}^{\mathrm{O}}\hat{\mathbf{j}}_{\mathrm{O}} = d_{A2} + (l_2 + E_1)\cos q_{21} - E_2\sin q_{21} \tag{3} $$

4. The $z_{\mathrm{O}}$ coordinate of point $B_2$ can be recognized as $(l_2 + E_1)\sin(q_{21}) + E_2\cos q_{21}$. Therefore, this condition can be expressed in terms of $\alpha$, $\theta$, $q_{21}$, $l_E$ and $l_2$ by:

$$ {}^{\mathrm{O}}_{\mathrm{F}}\mathbf{R}^{\mathrm{F}}\mathbf{r}_{B_2} \cdot {}^{\mathrm{O}}\hat{\mathbf{k}}_{\mathrm{O}} = (l_2 + E_1)\sin q_{21} + E_2\cos q_{21} \tag{4} $$

5. Points $E$ and $A_{2b}$ lie on a plane that is perpendicular to the $x_{\mathrm{E}}$ axis. It is known that ${}^{\mathrm{F}}\mathbf{r}_E = (-l_3, 0, l_1)$, while point $A_{2b}$ lies on the toroid:

$$ {}^{\mathrm{O}}\mathbf{r}_{A_{2b}} = d_{A2}{}^{\mathrm{O}}\hat{\mathbf{j}}_{\mathrm{O}} + \mathrm{Rot}(q_{21}, {}^{\mathrm{O}}\hat{\mathbf{i}}_{\mathrm{O}})\left[(0, E_1, E_2) - E_3\mathrm{Rot}(q_{22}, {}^{\mathrm{O}}\hat{\mathbf{k}}_{\mathrm{O}})^{\mathrm{O}}\hat{\mathbf{i}}_{\mathrm{O}}\right] $$

Therefore, this condition can be expressed in terms of $q_{11}$, $\theta$ and $l_3$ by:

$$ ({}^{\mathrm{F}}_{\mathrm{O}}\mathbf{R}^{\mathrm{O}}\mathbf{r}_{A_2} - {}^{\mathrm{F}}\mathbf{r}_E) \cdot {}^{\mathrm{F}}\hat{\mathbf{i}}_{\mathrm{F}} = 0 \tag{5} $$

6. $\mathscr{L}_T$ intersects $\mathbf{S}_{S1}$. It can be seen that $\mathscr{L}_T = \mathscr{L}(\hat{\mathbf{t}}, S')$ and $\mathbf{S}_{S1} = \mathscr{L}(\hat{\mathbf{k}}_{\mathrm{E}}, P_{S1})$, where ${}^{\mathrm{F}}\mathbf{r}_{P_{S1}} := (-l_3, h_y, 0)$. Therefore, this condition can be expressed in terms of $\theta$, $q_{11}$ and $l_3$ as:

$$ \left({}^{\mathrm{O}}\mathbf{r}_{S'} - {}^{\mathrm{O}}_{\mathrm{F}}\mathbf{R}^{\mathrm{F}}\mathbf{r}_{P_{S1}}\right) \cdot \left({}^{\mathrm{O}}\hat{\mathbf{t}} \times {}^{\mathrm{O}}\hat{\mathbf{k}}_{\mathrm{E}}\right) = 0 \tag{6} $$

Eqs. (1) to (6) represent a system of 8 scalar equations in 8 unknowns: $q_{11}$, $q_{21}$, $q_{22}$, $q_{S1}$, $\theta$, $l_1$, $l_2$ and $l_3$. We proceed now to reduce this system. The first component of vector Eq. (2) can be easily solved for $l_1$ to obtain:

$$ l_1 = \cos\theta(z_{S'}\cos q_{11} - y_{S'}\sin q_{11}) + x_{S'}\sin\theta - h_z \tag{7} $$

The third component of vector Eq. (2) can be solved for $l_3$ to obtain:

$$ l_3 = \sin\theta(z_{S'}\cos q_{11} - y_{S'}\sin q_{11}) - x_{S'}\cos\theta + d_S\sin q_{S1} \tag{8} $$

Eq. (4) can be solved for $l_2$ to obtain:

$$ l_2 = \frac{\cos q_{11}(l_3\sin\theta + l_1\cos\theta) + d_{B2}\sin q_{11} - E_2\cos q_{21}}{\sin q_{21}} - E_1 \tag{9} $$

The second component of Eq. (2) can be solved for $q_{S1}$ to obtain:

$$ q_{S1} = \pi \pm \arccos\left(\frac{z_{S'}\sin q_{11} + y_{S'}\cos q_{11} - h_y}{d_S}\right) \tag{10} $$

Substitution of these solutions in Eqs. (1), (3), (5) and (6) yields to two systems of 4 equations in the unknowns $q_{11}$, $q_{21}$, $q_{22}$ and $\theta$. Two systems are obtained due to the double solution for $q_{S1}$ in Eq. (10). The equations have no closed-form solution and have to be solved using numerical methods. Two solutions for the IKP are secured considering both systems of equations. The solutions can be distinguished by the "elbow up" and "elbow down" configurations of the serial module, although the configuration of the parallel differs too between solutions.

Once $q_{11}$, $q_{21}$, $q_{22}$ and $\theta$ is obtained, backwards substitution allows to obtain the other four variables, $\theta$, $l_3$, $l_1$ and $q_{S1}$. Frames E and F are now known as they only depend on $q_{11}$ and $\theta$. The actuation variables and coordinates of all joint screws can be obtained as expressions in terms of these five variables, and therefore, the IKP is solved.

Joint variables $q_{ij} \in \mathbb{R}$, $(i, j) \in \{(1,3), (2,4), (3,3)\}$ are given by $q_{ij} := |\mathbf{r}_{B_i/A_i}|$. To find the position of points $B_i$, we first locate $E$ w.r.t. frame O using ${}^{\mathrm{O}}\mathbf{r}_E = {}^{\mathrm{O}}_{\mathrm{F}}\mathbf{R}^{\mathrm{F}}\mathbf{r}_E = {}^{\mathrm{O}}_{\mathrm{F}}\mathbf{R}(-l_E, 0, h_E)$. Then,

$$ \begin{aligned} {}^{\mathrm{O}}\mathbf{r}_{B1} &= {}^{\mathrm{O}}\mathbf{r}_E + {}^{\mathrm{O}}_{\mathrm{E}}\mathbf{R}(d_{B1}, 0, 0) \\ {}^{\mathrm{O}}\mathbf{r}_{B2} &= {}^{\mathrm{O}}\mathbf{r}_E + {}^{\mathrm{O}}_{\mathrm{E}}\mathbf{R}(0, d_{B2}, 0) \\ {}^{\mathrm{O}}\mathbf{r}_{B3} &= {}^{\mathrm{O}}\mathbf{r}_E + {}^{\mathrm{O}}_{\mathrm{E}}\mathbf{R}(-d_{B1}, 0, 0) \end{aligned} \tag{11} $$

To find $q_{S2} \in \mathbb{T}$, we first consider the direction of $\mathbf{S}_{S2}$, ${}^{\mathrm{O}}\hat{\mathbf{s}}_{S2} = {}^{\mathrm{O}}_{\mathrm{E}}\mathbf{R}\mathrm{Rot}(q_{S1}, {}^{\mathrm{E}}\hat{\mathbf{k}}_{\mathrm{E}})^{\mathrm{E}}\hat{\mathbf{i}}_{\mathrm{E}}$. Then:

$$q_{S2} = \arctan2\left(\operatorname{sgn}\left(({}^{\mathrm{O}}\hat{\mathbf{k}}_{\mathrm{E}} \times {}^{\mathrm{O}}\hat{\mathbf{s}}_{S3}) \cdot {}^{\mathrm{O}}\hat{\mathbf{s}}_{S2}\right)\left|{}^{\mathrm{O}}\hat{\mathbf{k}}_{\mathrm{E}} \times {}^{\mathrm{O}}\hat{\mathbf{s}}_{S3}\right|, {}^{\mathrm{O}}\hat{\mathbf{k}}_{\mathrm{E}} \cdot {}^{\mathrm{O}}\hat{\mathbf{s}}_{S3}\right) \tag{12}$$

It is important to be aware that the system of equations presented here involves the location of four points $E$, $B_2$, $A_{2b}$ and $S'$. While the first three are permanently coplanar, $S'$ normally lies outside the plane that contains them, i.e. $y_E z_E$. This makes the system of equation solvable as all of its equations are independent to each other. However, if all four points become coplanar, then the system of equations cannot be solved. Note that such a situation happens whenever $q_{S1} \in \{0, \pi\} \Rightarrow \hat{\mathbf{s}}_{S2} \parallel \hat{\mathbf{i}}_E$. However, if this is the case, then we are able to compute $E$ in O with the input information of the IKP as ${}^{\mathrm{O}}\mathbf{r}_E = {}^{\mathrm{O}}\mathbf{r}_{S'} - (0, d_S + hy, h_z)$. Observe that it is the coordinate $x_{\mathrm{E}}$ of ${}^{\mathrm{E}}\mathbf{r}_{E/S'}$ which normally does not allows us to find $E$ with the input information, but in this case such a coordinate vanishes and $E$ is in hand. Since this is a point that is fixed to the moving platform, knowing ${}^{\mathrm{O}}\mathbf{r}_E$ allows us to decouple the robot and solve the IKP following the procedure presented in [17] if $E_i \neq 0$, or [14,16] if $E_i = 0$, $\forall i = 1, 2, 3$.

Although, in general, when solving systems of non-linear equations using software it is necessary to provide either an initial guess or bounds for the variables, the process can be automated by using as initial guess the solution for the IKP of the robot with spherical wrist and no offsets, since the latter has a closed-form solution that is also unique within the joint limits. This initial guess is not far away from the solution of our non-linear system of equations as the offsets ($E_i$ and $d_S$) will always be small compared to the dimensions of the robot. The solution for the IKP of the Exechon robot with spherical wrist and no offsets can be found in [14,16].

### 4.1. IKP for the Exechon robot with offset wrist and nominal dimensions

If $E_i = 0$ for $i = 1, \ldots, 5$, but $d_S \neq 0$, the IKP still cannot be decoupled, but the solution can be reduced to a single polynomial equation.

The substitution $E_i = 0$, $\forall i = 1, \ldots, 5$ considerably simplifies Eq. (5) since point $A_{2b}$ is now fixed, no longer lying on a toroid, so ${}^{\mathrm{O}}\mathbf{r}_{A_{2b}} = (0, d_{A2}, 0)$. Such a substitution does not affect Eqs. (2) and (6), which, together with our new simplified Eq. (5), represent a system of equation of 5 equations in 5 unknowns: $\theta$, $q_{11}$, $l_1$, $l_3$ and $q_{S1}$.

Eq. (5) and the third component of Eq. (2) are linear on $l_3$ and $l_1$, respectively, and can be solved for these variables.

The first and second components of Eq. (2) can be combined to eliminate $q_{S1}$, obtaining the following equation:

$$(x_{S'}\cos\theta + y_{S'}\sin\alpha\sin\theta - z_{S'}\cos\alpha\sin\theta + l_3)^2 + (y_{S'}\cos\alpha + z_{S'}\sin\alpha - h_y)^2 = d_S^2 \tag{13}$$

The expressions for $l_3$ and $l_1$ obtained from Eq. (5) and the third component of Eq. (2), respectively, are then replaced in Eqs. (6) and (13). After this substitution, Eqs. (6) and (13) become a system of two equations in $q_{11}$ and $\theta$. Eq. (6) can be solved for $\theta$ to obtain:

$$\theta = \arctan\frac{(x_{S'}t_3 - z_{S'}t_1)\sin\alpha + (x_{S'}t_2 - y_{S'}t_1)\cos\alpha + h_y t_1}{(d_{A2}(t_3\sin\alpha + t_2\cos\alpha) - h_y t_2)\sin\alpha + h_y t_3\cos\alpha - t_3 y_{S'} + t_2 z_{S'}} \tag{14}$$

Substituting Eq. (14) into Eq. (13), a single equation in $q_{11}$ is obtained. By using the tangent half-angle substitution, such expression can be reduced to a polynomial of degree 16, this results coincides with the expected polynomial for manipulators with offset wrists [18].

## 5. Systems of constraints and actuations

In this section, the systems of constraints and actuations of the Exechon robot with offset wrist and offsets in the joints connecting the legs to the fixed platform are determined. Since for the stiffness analysis the serial module and the parallel module are considered as two elements connected serially, the systems of constraints and actuations of each module are obtained separately. The presence of offsets $E_4$ and $E_5$ in legs 1 and 3 does not have any significant effect on the systems of constraints and actuations of the ideal model. These can be found in the literature [12]. However, for the sake of self-containment, such systems are determined here as well.

Let the coordinates of any (unit) screw be given by $\mathbf{S} := (\hat{\mathbf{s}}; \mathbf{r} \times \hat{\mathbf{s}} + h\hat{\mathbf{s}}) \in \mathrm{se}(3) \cong \mathbb{R}^6$, $\hat{\mathbf{s}} \in \mathbb{S}^2$, $\mathbf{r} \in \mathbb{R}^3$, $h \in \mathbb{R}$. Then a twist is given by $\mathbf{V} := \omega\mathbf{S} = (\boldsymbol{\omega}; \mathbf{v})$ and a wrench by $\mathbf{W} := (\mathbf{f}; \mathbf{m})$. We invert the components of a screw using $\tilde{\mathbf{S}} := (\mathbf{r} \times \hat{\mathbf{s}} + h\hat{\mathbf{s}}; \hat{\mathbf{s}})$.

If $\mathscr{S}_i := \mathrm{span}(\mathbf{s}_{i1}, \ldots, \mathbf{s}_{in})$, then the system of constraints of leg $i$ is given by $\mathscr{W}_{ci} := \{\mathbf{W}_{cij} : \mathrm{kl}(\mathbf{W}_{cij}, \mathbf{S}) = 0, \forall \mathbf{S} \in \mathscr{S}_i\}$, where $\mathrm{kl}(\mathbf{S}_1, \mathbf{S}_2) = (\tilde{\mathbf{S}}_1)^{\mathrm{t}}\mathbf{S}_2$ is the Klein form in se(3). The constraint system of the moving platform is then given by the sum of the constraint systems of each leg.

A basis for the constraints system of each leg is shown in Fig. 4. For legs $i = 1, 3$ it follows $\mathscr{W}_{ci} := \mathrm{span}(\mathbf{W}_{ci1}, \mathbf{W}_{ci2})$, where $\mathbf{W}_{ci1}$ is a pure moment with direction perpendicular to $\hat{\mathbf{S}}_{i1}$ and $\hat{\mathbf{S}}_{i2}$, while $\mathbf{W}_{ci2}$ is a pure force that is parallel to $\hat{\mathbf{S}}_{i4}$ and intersects $\mathbf{S}_{i1}$:

$$\begin{aligned} {}^{\mathrm{O}}\mathbf{W}_{ci1} &= \left(\mathbf{0}; {}^{\mathrm{O}}\hat{\mathbf{i}}_{\mathrm{O}} \times {}^{\mathrm{O}}\hat{\mathbf{j}}_{\mathrm{F}}\right), \\ {}^{\mathrm{O}}\mathbf{W}_{ci2} &= \left({}^{\mathrm{O}}\hat{\mathbf{j}}_{\mathrm{E}}; {}^{\mathrm{O}}\mathbf{r}_{A_{ia}} \times {}^{\mathrm{O}}\hat{\mathbf{j}}_{\mathrm{E}}\right), \end{aligned} \tag{15}$$

The offsets between joint axes in leg 2 do not the determination of ${}^{\mathrm{O}}\mathbf{W}_{c21}$, the single wrench in the basis of $\mathscr{W}_2$, by simple geometric means. As shown in [17], ${}^{\mathrm{O}}\mathbf{W}_{c21}$ can be found by computation of a basis for $\mathrm{Null}((\mathbf{J}_2(\mathbf{q}))^{\mathrm{t}}) = \mathrm{span}({}^{\mathrm{O}}\tilde{\mathbf{W}}_{c21})$, where $\mathbf{J}_2 := \mathrm{aug}({}^{\mathrm{O}}\mathbf{S}_{21}, \ldots, {}^{\mathrm{O}}\mathbf{S}_{25})$. Clearly, $\dim(\mathrm{Null}((\mathbf{J}_2(\mathbf{q}))^{\mathrm{t}})) = 1$. This null space can be computed directly using the function `nullspace`

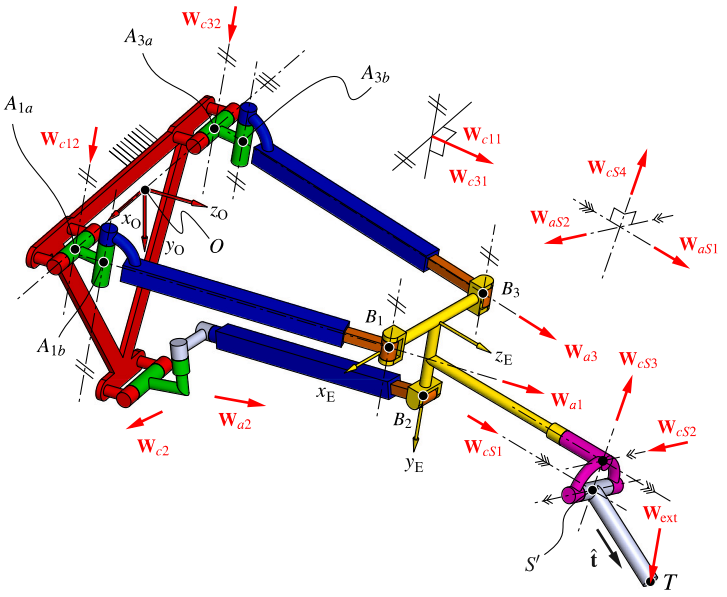


**Fig. 4.** System of constraints and system of actuations.

of Maple©. In general, $\mathbf{W}_{c21}$ is neither a pure force, nor a pure moment. However, in the case of $E_1 = E_2 = E_3 = 0$, the wrench degenerates into a pure force ${}^{O}\mathbf{W}_{c2} = \left({}^{O}\hat{\mathbf{i}}_E; {}^{O}\mathbf{r}_{A_{2a}} \times {}^{O}\hat{\mathbf{i}}_E\right)$

The twist of the moving platform with respect to the fixed one, $\mathbf{V}_{mp} \in se(3)$, is given by

$$\mathbf{V}_{mp} := \sum_{j=1}^{4} \dot{q}_{1j}\mathbf{S}_{1j} = \sum_{j=1}^{5} \dot{q}_{2j}\mathbf{S}_{2j} = \sum_{j=1}^{4} \dot{q}_{3j}\mathbf{S}_{3j}$$

Without loss of generality, for leg 1, for example, it follows:

$$\mathrm{kl}\left(\sum_{j=1}^{4} \dot{q}_{1j}\mathbf{S}_{1j},\, \mathbf{W}_{c1k}\right) = 0 \;\Rightarrow\; \left(\sum_{j=1}^{4} \dot{q}_{1j}\mathbf{S}_{1j}\right)^{\mathrm{t}} \tilde{\mathbf{W}}_{c1k} = 0,\; k = 1,2 \tag{16}$$

Considering Eq. (16) for all legs, the expression $\mathbf{J}_{Pc}\mathbf{V}_{mp} = \mathbf{0}$ can be written, where $\mathbf{J}_{Pc} \in \mathbb{R}^{5\times 6}$ is the Jacobian of constraints and is given by:

$$\mathbf{J}_{Pc} := \mathrm{aug}\left(\tilde{\mathbf{W}}_{c11}, \tilde{\mathbf{W}}_{c12}, \tilde{\mathbf{W}}_{c2}, \tilde{\mathbf{W}}_{c31}, \tilde{\mathbf{W}}_{c32}\right)^{\mathrm{t}}$$

Now consider the wrenches of actuation $\mathbf{W}_{ai}$, $i = 1,2,3$, for which $\mathrm{kl}(\mathbf{W}_{ai}, \mathbf{S}_{ij}) = 0$ if joint $ij$ is not actuated and $\mathrm{kl}(\mathbf{W}_{ai}, \mathbf{S}_{ij}) \neq 0$ if joint $ij$ is the actuated joint of leg $i$. Without loss of generality, for leg 1 it follows:

$$\mathrm{kl}\left(\sum_{j=1}^{4} \dot{q}_{1j}\mathbf{S}_{1j},\, \mathbf{W}_{a1}\right) = \dot{q}_{13}\mathrm{kl}(\mathbf{S}_{13}, \mathbf{W}_{a1})$$
$$\Rightarrow \mathbf{V}_{mp}^{\mathrm{t}}\tilde{\mathbf{W}}_{a1} = \dot{q}_{13}\mathrm{kl}(\mathbf{S}_{13}, \mathbf{W}_{a1}) \tag{17}$$

Considering Eq. (17) for all legs, the expression $\mathbf{J}_{Pa}\mathbf{V}_{mp} = (\dot{q}_{13}, \dot{q}_{24}, \dot{q}_{33})$ can be written, where $\mathbf{J}_{Pa} \in \mathbb{R}^{3\times 6}$ is the Jacobian of actuations and is given by:

$$\mathbf{J}_{Pa} := \mathrm{aug}\left(\frac{\tilde{\mathbf{W}}_{a1}}{\mathrm{kl}(\mathbf{S}_{13}, \mathbf{W}_{a1})}, \frac{\tilde{\mathbf{W}}_{a2}}{\mathrm{kl}(\mathbf{S}_{24}, \mathbf{W}_{a2})}, \frac{\tilde{\mathbf{W}}_{a3}}{\mathrm{kl}(\mathbf{S}_{33}, \mathbf{W}_{a3})}\right)^{\mathrm{t}}$$

where,

$${}^{O}\mathbf{W}_{ai} = \left(\frac{{}^{O}\mathbf{r}_{B_i/A_{ib}}}{|{}^{O}\mathbf{r}_{B_i/A_{ib}}|}; {}^{O}\mathbf{r}_{A_{ib}} \times {}^{O}\mathbf{r}_{B_i/A_{ib}}\right),\; i = 1,3 \tag{18}$$

For leg 2, there is again no direct geometric method to determine ${}^{O}\mathbf{W}_{a2}$. However, let $\mathbf{J}_2^* := \mathrm{aug}({}^{O}\mathbf{S}_{21}, {}^{O}\mathbf{S}_{22}, {}^{O}\mathbf{S}_{23}, {}^{O}\mathbf{S}_{25})$, then we note that ${}^{O}\tilde{\mathbf{W}}_{a2} \in \mathrm{Null}((\mathbf{J}_2^*)^{\mathrm{t}})$, but ${}^{O}\tilde{\mathbf{W}}_{a2} \notin \mathrm{Null}(\mathbf{J}_2^{\mathrm{t}})$. It is clear that $\mathrm{Null}(\mathbf{J}_2^{\mathrm{t}}) < \mathrm{Null}((\mathbf{J}_2^*)^{\mathrm{t}})$. Therefore, a simple way to find ${}^{O}\mathbf{W}_{a2}$ is to obtain bases for both null spaces. Since $\dim(\mathrm{Null}((\mathbf{J}_2^*)^{\mathrm{t}})) = 2$, one can pick any of the two vectors in its basis and verify that it is not

parallel to ${}^{O}\tilde{\mathbf{W}}_{c2}$. If the wrenches are not parallel, then such a vector can be taken as ${}^{O}\tilde{\mathbf{W}}_{a2}$. In the case of $E_1 = E_2 = E_3 = 0$, ${}^{O}\tilde{\mathbf{W}}_{a2}$ is reduced to a pure force along the actuator axis and can be computed making $i = 2$ in Eq. (18).

A similar analysis can be done for the 2-DOF serial module to obtain the following Jacobians of constraints and actuations:

$$\begin{aligned}\mathbf{J}_{Pc} &:= \text{aug}\left(\tilde{\mathbf{W}}_{cS1}, \tilde{\mathbf{W}}_{cS2}, \tilde{\mathbf{W}}_{cS3}, \tilde{\mathbf{W}}_{cS4}\right)^{\mathrm{t}},\\ \mathbf{J}_{Pa} &:= \text{aug}\left(\tilde{\mathbf{W}}_{aS1}, \tilde{\mathbf{W}}_{aS2}\right)^{\mathrm{t}}\end{aligned} \tag{19}$$

where,

$$\begin{aligned}{}^{O}\mathbf{W}_{cS1} &= \left({}^{O}\hat{\mathbf{k}}_{E}; {}^{O}\mathbf{r}_{S'} \times {}^{O}\hat{\mathbf{k}}_{E}\right),\\ {}^{O}\mathbf{W}_{cS2} &= \left({}^{O}\hat{\mathbf{s}}_{S2}; {}^{O}\mathbf{r}_{P_{S1}} \times {}^{O}\hat{\mathbf{s}}_{S2}\right),\\ {}^{O}\mathbf{W}_{cS3} &= \left({}^{O}\hat{\mathbf{k}}_{E} \times {}^{O}\hat{\mathbf{s}}_{S2}; {}^{O}\mathbf{r}_{S'} \times ({}^{O}\hat{\mathbf{k}}_{E} \times {}^{O}\hat{\mathbf{s}}_{S2})\right),\\ {}^{O}\mathbf{W}_{cS4} &= \left(\mathbf{0}; {}^{O}\hat{\mathbf{k}}_{E} \times {}^{O}\hat{\mathbf{s}}_{S2}\right),\\ {}^{O}\mathbf{W}_{aS1} &= \left(\mathbf{0}; {}^{O}\hat{\mathbf{k}}_{E}\right),\\ {}^{O}\mathbf{W}_{aS2} &= \left(\mathbf{0}; {}^{O}\hat{\mathbf{s}}_{S2}\right)\end{aligned} \tag{20}$$

where ${}^{O}\hat{\mathbf{s}}_{S2} = \text{Rot}(q_{S1}, {}^{E}\hat{\mathbf{k}}_{E}){}^{E}\hat{\mathbf{i}}_{E}$. The *overall* Jacobian matrices [22] for the parallel and serial modules are given, respectively, by:

$$\mathbf{J}_P := \begin{bmatrix} \mathbf{J}_{Pa} \\ \mathbf{J}_{Pc} \end{bmatrix} \in \mathbb{R}^{8\times 6},\ \mathbf{J}_S := \begin{bmatrix} \mathbf{J}_{Sa} \\ \mathbf{J}_{Sc} \end{bmatrix} \in \mathbb{R}^{6\times 6},$$

## 6. Compliance equation for the hybrid manipulator case

Let T be a coordinate system that is parallel to frame O but has origin at $T$. We now refer the coordinates of every wrench in $\mathbf{J}_{Pc}$, $\mathbf{J}_{Pa}$, $\mathbf{J}_{Sc}$ and $\mathbf{J}_{Sa}$ to frame T by means of ${}^{T}\mathbf{W} = \text{Adj}(\text{id}_{SO(3)}, {}^{O}\mathbf{r}_{T})^{O}\mathbf{W}$. Once all Jacobians are expressed in frame T, the compliance matrix of the whole system can be expressed as the sum of the compliance matrix of the parallel module and the compliance matrix of the serial module.

The proof of the stiffness equations for both the parallel and the serial cases is included in several publications with equivalent results (see [12,13,19]). Only the resulting expressions will be included in this article.

Let ${}^{T}\mathbf{W}_{\text{ext}}$ be the external wrench applied at $T$ and let ${}^{T}\Delta\mathbf{X} := (\Delta\theta; \Delta\mathbf{r}_{T})$ be the deformation at $T$. The applied wrench and the corresponding deformation are then related by:

$${}^{T}\Delta\mathbf{X} = \left(\mathbf{C}_P + \mathbf{C}_S\right){}^{T}\tilde{\mathbf{W}}_{\text{ext}} \tag{21}$$

where $\mathbf{C}_P$ and $\mathbf{C}_S$ are the compliance matrices of the parallel and the serial module, respectively, and are given by:

$$\mathbf{C}_P := \left(\mathbf{J}_P^{\mathrm{t}}(\overline{\mathbf{C}}_P)^{-1}\mathbf{J}_P\right)^{-1},\ \mathbf{C}_S := \left(\mathbf{J}_S^{\mathrm{t}}(\overline{\mathbf{C}}_S)^{-1}\mathbf{J}_S\right)^{-1}, \tag{22}$$

where the entries of $\overline{\mathbf{C}}_P$ and $\overline{\mathbf{C}}_S$, are the compliances in the directions of actuations and constraints, such that, without loss of generality, for the parallel module $\Delta\mathbf{q}_P = \overline{\mathbf{C}}_P\boldsymbol{\tau}_P$. Where $\Delta\mathbf{q}_P := (\Delta q_{a1}, \Delta q_{a2}, \Delta q_{a3}, \Delta q_{c11}, \Delta q_{c12}, \Delta q_{c2}, \Delta q_{c31}, \Delta q_{c32})$ is the vector of displacements along the actuations and constraints directions, and $\boldsymbol{\tau}_P := (\tau_{a1}, \tau_{a2}, \tau_{a3}, \tau_{c11}, \tau_{c12}, \tau_{c2}, \tau_{c31}, \tau_{c32})$ are the forces/moments applied in the directions of constraints and actuations. The following notation is used for the entries of $\overline{\mathbf{C}}_P$ and $\overline{\mathbf{C}}_S$: For example, the diagonal element in the 4th row and 4th column represents the compliance in the direction of constraint $q_{c11}$ due to the application of a moment $\tau_{c11}$ in the same direction and it is referred to as $c_{c11}^{c11}$. Outside the diagonal, the element in the 4th row and 5th column is the compliance in the direction of $q_{c11}$ due to the application of a force $\tau_{c12}$ and it is referred to as $c_{c11}^{c12}$. It can be seen that this last example is a coupled compliance and, due to the linear nature of the deformations in the model, $c_{c12}^{c11} = c_{c11}^{c12}$.

As shown in Eq. (6), the resulting compliance matrix of two elements connected serially is the sum of their respective compliance matrices. This is why in this paper we work with compliance matrices instead of stiffness, which would involve the calculation of inverses in Eq. (6), in order to obtain the obtained displacement. Hence, this is a common practice when dealing with serially-connected modules, see [13,33].

## 7. Elements in $\overline{\mathbf{C}}_P$ and $\overline{\mathbf{C}}_S$

In this section, the entries of $\overline{\mathbf{C}}_P$ and $\overline{\mathbf{C}}_S$ are discussed. We construct such matrices the following way:

$$\begin{aligned}\overline{\mathbf{C}}_P &= \text{diag}\left(c_{a1}^{a1}, c_{a2}^{a2}, c_{a3}^{a3}, c_{c11}^{c11}, c_{c12}^{c12}, c_{c2}^{c2}, c_{c31}^{c31}, c_{c32}^{c32}\right)\\ \overline{\mathbf{C}}_S &= \text{diag}\left(c_{aS1}^{aS1}, c_{aS2}^{aS2}, c_{cS1}^{cS1}, c_{cS2}^{cS2}, c_{cS3}^{cS3}, c_{cS4}^{cS4}\right)\end{aligned}$$

Since these entries depend on the specifications of each robot, the case of the Exechon XMini is treated here. In the nominal dimensions of the XMini model, $E_i = 0$, $\forall i = 1, \ldots, 5$, however, the serial module is an offset wrist, as shown in Fig. 1, so that $d_S = 50$ mm $\neq 0$. The following analysis can be applied to any model with these offsets characteristics.

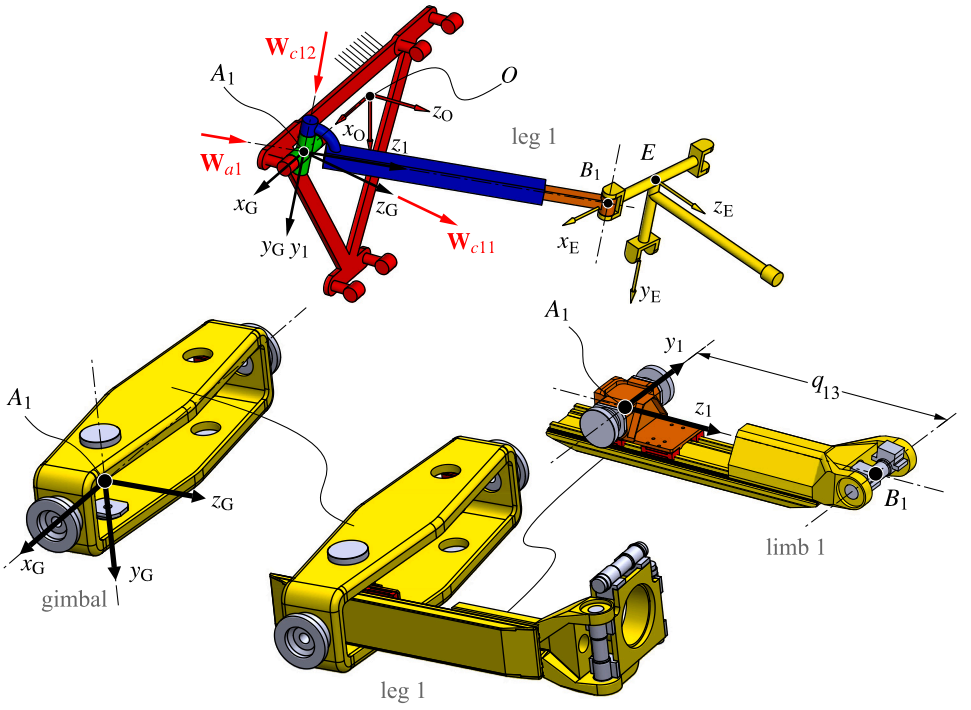


**Fig. 5.** Components and coordinate systems in leg 1.

For this analysis, several coordinate systems with coincident origins are established and compliances are expressed in different frames by means of a transformation of coordinate systems [13,19,34]. For example, if the linear compliance matrix of an element is known in frame A and we would like to know the linear compliance along a vector $\hat{\mathbf{u}}$, which is known in frame B, then such a compliance is given by $c_{\Lambda,\hat{\mathbf{u}}} = ({}^{\mathrm{B}}\hat{\mathbf{u}})^{\mathrm{t}} \cdot {}^{\mathrm{B}}_{\mathrm{A}}\mathbf{R} \cdot \mathbf{C}_{\Lambda} \cdot {}^{\mathrm{A}}_{\mathrm{B}}\mathbf{R} \cdot {}^{\mathrm{B}}\hat{\mathbf{u}}$, where $\mathbf{C}_{\Lambda}$ is the linear compliance matrix in frame A. We will use $\Lambda$ and $\Theta$ to distinguish between linear and torsional compliances. Also note that *only* in this section, we will be using $(\cdot)$ to represent matrix multiplication instead of dot product, this is due to the amount of subscripts and superscripts for which juxtaposition may lead to confusion.

### 7.1. Legs 1 and 3

Since $E_4 = E_5 = 0$, we define $A_i = A_{ia} = A_{ib}$, for $i = 1, 3$. Then we establish a coordinate system $i$ with origin at $A_i$, $z_i$ axis in the direction of $\mathbf{r}_{B_i/A_i}$ and $y_i$ axis in the direction of $\hat{\mathbf{s}}_{i2} = \hat{\mathbf{j}}_{\mathrm{E}}$ as shown in Fig. 5. Frame $i$ is fixed to the slider. We also define coordinate system G, which shares the same origin and $y$ axis as $i$ but, its $x_{\mathrm{G}}$ axis is in the direction of $x_{\mathrm{O}}$. Frame G is fixed to the gimbal. An abuse of notation will be committed here as we will call simply G this last frame for both legs, although in each leg frame G has a different origin.

For this model, legs $i = 1, 3$ are disassembled in two parts shown in Fig. 5, we call this elements "gimbal" and "limb $i$". Element limb $i$ encompasses the rail, slider, bearings, screw lead and other components. Note that we use "leg" to refer to the entire kinematic chain from base to moving platform, while "limb" denotes the element just defined.

From the constraints and actuations system shown in Fig. 5, the compliance of the gimbal in all the directions of the wrenches in these two systems can be obtained by simple projection of the fixed-value linear and torsional compliance matrices in frame G, $\mathbf{C}_{\Lambda,\mathrm{gim}}$ and $\mathbf{C}_{\Theta,\mathrm{gim}}$, respectively. Such matrices are determined using FEM. It follows that:

$$
\begin{aligned}
c^{ai}_{ai,\mathrm{gim}} &= ({}^{i}\hat{\mathbf{k}}_i)^{\mathrm{t}} \cdot {}^{i}_{\mathrm{G}}\mathbf{R} \cdot \mathbf{C}_{\Lambda,\mathrm{gim}} \cdot {}^{\mathrm{G}}_{i}\mathbf{R} \cdot {}^{i}\hat{\mathbf{k}}_i \\
c^{ci1}_{ci1,\mathrm{gim}} &= ({}^{\mathrm{G}}\hat{\mathbf{k}}_{\mathrm{G}})^{\mathrm{t}} \cdot \mathbf{I}_{3\times3} \cdot \mathbf{C}_{\Theta,\mathrm{gim}} \cdot \mathbf{I}_{3\times3} \cdot {}^{\mathrm{G}}\hat{\mathbf{k}}_{\mathrm{G}} \\
c^{ci2}_{ci2,\mathrm{gim}} &= ({}^{\mathrm{G}}\hat{\mathbf{j}}_{\mathrm{G}})^{\mathrm{t}} \cdot \mathbf{I}_{3\times3} \cdot \mathbf{C}_{\Lambda,\mathrm{gim}} \cdot \mathbf{I}_{3\times3} \cdot {}^{\mathrm{G}}\hat{\mathbf{j}}_{\mathrm{G}}
\end{aligned}
$$

The entries of the compliance matrices of element limb $i$ in frame $i$ are modeled considering a quadratic and a linear term in the leg length, $q_{i3}$:

$$
\mathbf{C}_{\Lambda,\mathrm{lim}i} = \mathrm{diag}\left( \sum_{j=1}^{2} k_{\Lambda,x,j} q_{i3}^{j}, \sum_{j=1}^{2} k_{\Lambda,y,j} q_{i3}^{j}, \sum_{j=1}^{2} k_{\Lambda,z,j} q_{i3}^{j} \right)
$$

$$\mathbf{C}_{\Theta,\text{lim}i} = \text{diag}\left(\sum_{j=1}^{2} k_{\Theta,x,j} q_{i3}^{j}, \sum_{j=1}^{2} k_{\Theta,y,j} q_{i3}^{j}, \sum_{j=1}^{2} k_{\Theta,z,j} q_{i3}^{j}\right) \tag{23}$$

where $k_{\Lambda,a,j}$, $k_{\Theta,a,j} \in \mathbb{R}$, $a = x, y, z$ and $j = 1, 2$, are the coefficients of the polynomials. Note that these coefficients are not directly related to any geometrical or mechanical property of the element, they are rather a means to model such properties.

It follows that:

$$\begin{aligned}
c_{ai,\text{lim}i}^{ai} &= ({}^{i}\hat{\mathbf{k}}_i)^{\text{t}} \cdot \mathbf{I}_{3\times3} \cdot \mathbf{C}_{\Lambda,\text{lim}i} \cdot \mathbf{I}_{3\times3} \cdot {}^{i}\hat{\mathbf{k}}_i \\
c_{ci1,\text{lim}i}^{ci1} &= ({}^{\text{G}}\hat{\mathbf{k}}_{\text{G}})^{\text{t}} \cdot {}^{\text{G}}_{i}\mathbf{R} \cdot \mathbf{C}_{\Theta,\text{lim}i} \cdot {}^{i}_{\text{G}}\mathbf{R} \cdot {}^{\text{G}}\hat{\mathbf{k}}_{\text{G}} \\
c_{ci2,\text{lim}i}^{ci2} &= ({}^{i}\hat{\mathbf{j}}_i)^{\text{t}} \cdot \mathbf{I}_{3\times3} \cdot \mathbf{C}_{\Lambda,\text{lim}i} \cdot \mathbf{I}_{3\times3} \cdot {}^{i}\hat{\mathbf{j}}_i
\end{aligned} \tag{24}$$

The compliance of each element and the compliance of the actuator, $c_{\text{act}}$, contribute to the compliance of the entire leg, hence:

$$\begin{aligned}
c_{ai}^{ai} &= c_{ai,\text{lim}i}^{ai} + c_{ai,\text{gim}}^{ai} + c_{\text{act}} \\
c_{ci1}^{ci1} &= c_{ci1,\text{lim}i}^{ci1} + c_{ci1,\text{gim}}^{ci1} \\
c_{ci2}^{ci2} &= c_{ci2,\text{lim}i}^{ci2} + c_{ci2,\text{gim}}^{ci2}
\end{aligned}$$

Coupled compliance $c_{ci2}^{ci1} = c_{ci1}^{ci2}$ is ignored.

The components whose compliance is computed using FEM are individually modeled based on its geometry and materials. Then a known force or torque is applied at the joint or connection assuming the force is derived from other part.

### 7.2. Legs 2

For this model, leg 2 is disassembled in the parts shown in Fig. 6: "gimbal 1", "gimbal 2", "axis 2" and an element "limb 2" encompassing the rail, slider, bearings, screw lead and other components.

Since $E_1 = E_2 = E_3 = 0$, we define $A_2 = A_{2a} = A_{2b} = A_{2c}$. Then we establish a coordinate system 2 with origin at $A_2$, $z_2$ axis in the direction of $\mathbf{r}_{B_2/A_2}$ and $y_2$ axis in the direction of $\hat{\mathbf{s}}_{25} = \hat{\mathbf{i}}_{\text{E}}$ as shown in Fig. 6. Frame 2 is attached to the slider.

A coordinate system is fixed to each of the two gimbals of the spherical joint of leg 2. Frame G1 is attached to gimbal 1, and G2 to elements gimbal 2 and axis 2. These two frames have the same origin, point $A_2$ and are defined by:

$$\begin{aligned}
{}^{\text{O}}_{\text{G1}}\mathbf{R} &:= \text{Rot}\left(q_{21} - \frac{\pi}{2}, {}^{\text{O}}\hat{\mathbf{i}}_{\text{O}}\right) \\
{}^{\text{G1}}_{\text{G2}}\mathbf{R} &:= \text{Rot}\left(\frac{\pi}{2} - q_{22}, {}^{\text{G1}}\hat{\mathbf{j}}_{\text{G1}}\right)
\end{aligned}$$

Note that, since $E_1 = E_2 = E_3 = 0$, the bases for the systems of constraints and actuations are reduced to the two pure forces shown in Fig. 6. Hence, only linear compliance matrices are required. The compliance of element gimbal 1 in all the directions of the wrenches in these two systems can be obtained by simple projection of the fixed-value linear compliance matrix in frame G1, $\mathbf{C}_{\Lambda,\text{gim1}}$. Similarly, for elements gimbal 2 and axis 2, the required compliances can be obtained by projecting the fixed-value linear compliance matrix in frame G2, $\mathbf{C}_{\Lambda,\text{gim2}}$ and $\mathbf{C}_{\Lambda,\text{ax2}}$, respectively. These three matrices are determined using FEM. It follows that:

$$\begin{aligned}
c_{a2,\text{gim1}}^{a2} &= ({}^{\text{O}}\hat{\mathbf{w}}_{a2})^{\text{t}} \cdot {}^{\text{O}}_{\text{G1}}\mathbf{R} \cdot \mathbf{C}_{\Lambda,\text{gim1}} \cdot {}^{\text{G1}}_{\text{O}}\mathbf{R} \cdot {}^{\text{O}}\hat{\mathbf{w}}_{a2} \\
c_{c2,\text{gim1}}^{c2} &= ({}^{\text{O}}\hat{\mathbf{w}}_{c2})^{\text{t}} \cdot {}^{\text{O}}_{\text{G1}}\mathbf{R} \cdot \mathbf{C}_{\Lambda,\text{gim1}} \cdot {}^{\text{G1}}_{\text{O}}\mathbf{R} \cdot {}^{\text{O}}\hat{\mathbf{w}}_{c2} \\
c_{a2,\text{gim2}}^{a2} &= ({}^{\text{G2}}\hat{\mathbf{i}}_{\text{G2}})^{\text{t}} \cdot \mathbf{I}_{3\times3} \cdot \mathbf{C}_{\Lambda,\text{gim2}} \cdot {}^{\text{G2}}_{\text{O}} \cdot \mathbf{I}_{3\times3} \cdot {}^{\text{G2}}\hat{\mathbf{i}}_{\text{G2}} \\
c_{c2,\text{gim2}}^{c2} &= ({}^{\text{O}}\hat{\mathbf{w}}_{c2})^{\text{t}} \cdot {}^{\text{O}}_{\text{G2}}\mathbf{R} \cdot \mathbf{C}_{\Lambda,\text{gim2}} \cdot {}^{\text{G2}}_{\text{O}}\mathbf{R} \cdot {}^{\text{O}}\hat{\mathbf{w}}_{c2} \\
c_{a2,\text{ax2}}^{a2} &= ({}^{\text{G2}}\hat{\mathbf{i}}_{\text{G2}})^{\text{t}} \cdot \mathbf{I}_{3\times3} \cdot \mathbf{C}_{\Lambda,\text{ax2}} \cdot {}^{\text{G2}}_{\text{O}} \cdot \mathbf{I}_{3\times3} \cdot {}^{\text{G2}}\hat{\mathbf{i}}_{\text{G2}} \\
c_{c2,\text{ax2}}^{c2} &= ({}^{\text{O}}\hat{\mathbf{w}}_{c2})^{\text{t}} \cdot {}^{\text{O}}_{\text{G2}}\mathbf{R} \cdot \mathbf{C}_{\Lambda,\text{ax2}} \cdot {}^{\text{G2}}_{\text{O}}\mathbf{R} \cdot {}^{\text{O}}\hat{\mathbf{w}}_{a2}
\end{aligned}$$

The same model from Eq. (23) is used for the compliance matrices of the leg element limb 2 in frame 2. Hence, $\mathbf{C}_{\Lambda,\text{lim2}}$ and $\mathbf{C}_{\Theta,\text{lim2}}$ are obtained by substituting $q_{i3}$ by $q_{24}$ in Eq. (23). It follows that:

$$\begin{aligned}
c_{a2,\text{lim2}}^{a2} &= ({}^{2}\hat{\mathbf{k}}_2)^{\text{t}} \cdot \mathbf{I}_{3\times3} \cdot \mathbf{C}_{\Lambda,\text{leg2}} \cdot \mathbf{I}_{3\times3} \cdot {}^{2}\hat{\mathbf{k}}_2 \\
c_{c2,\text{lim2}}^{c2} &= ({}^{2}\hat{\mathbf{j}}_2)^{\text{t}} \cdot \mathbf{I}_{3\times3} \cdot \mathbf{C}_{\Lambda,\text{leg2}} \cdot \mathbf{I}_{3\times3}^{2} \cdot \hat{\mathbf{j}}_2
\end{aligned} \tag{25}$$

The compliance of each element and the compliance of the actuator, $c_{\text{act}}$, contribute to the compliance of the entire leg, hence:

$$\begin{aligned}
c_{a2}^{a2} &= c_{a2,\text{lim2}}^{a2} + c_{a2,\text{gim1}}^{a2} + c_{a2,\text{gim2}}^{a2} + c_{a2,\text{ax2}}^{a2} + c_{\text{act}} \\
c_{c2}^{c2} &= c_{c2,\text{lim2}}^{c2} + c_{c2,\text{gim1}}^{c2} + c_{c2,\text{gim2}}^{c2} + + c_{c2,\text{ax2}}^{c2}
\end{aligned}$$

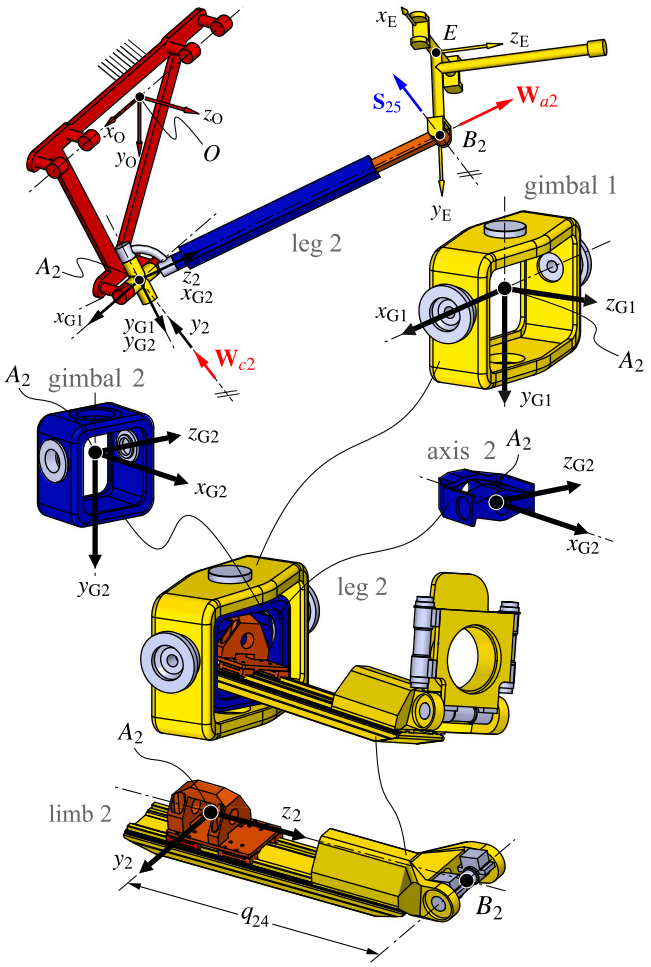


**Fig. 6.** Components and coordinate systems in leg 2.

### 7.3. Serial module

For this model, only the main body of the serial module is considered as compliant since the link connecting actuator $S2$ and the spindle is mainly the body of the motor of the tool. From Fig. 7, it can be seen that all the wrenches of constraints and actuations have constant directions with respect to the main body of the serial model, link $S1 - S2$. Hence, all the compliances for the serial part are constant and are assumed to be decoupled. The values of constraint compliances $c_{cSi}^{cSi}$, $i = 1, \ldots, 4$, are obtained from FEA. $c_{aS1}^{aS1}$ and $c_{aS2}^{aS2}$ correspond to the compliance of actuators of the serial module and they include not only the compliance of the motors, but also that of its transmission system.

## 8. Finding unknown coefficients from experimental data

The model presented in Section 7 is in terms of several constants that can be obtained from FEM in the case of elements whose compliance can be obtained by projecting the fixed compliance matrix in a local frame. However, the compliance of leg elements e1, e2 and e3, modeled in the form of Eq. (23), is in terms of the unknown polynomial coefficients $k_{\Lambda,a,j}, k_{\Theta,a,j} \in \mathbb{R}$, $a = x, y, z$ and $j = 0, 1, 2$. In addition, the compliance values of all the actuators, namely $c_{\text{act}}$, $c_{aS1}^{aS1}$ and $c_{aS2}^{aS2}$, are also unknown. However, an inspection of the systems of constraint and actuation in Figs. 5 and 6 shows that the $x$ component of $\mathbf{C}_{\Lambda,\text{lim}i}$ and the $y$ component of $\mathbf{C}_{\Lambda,\text{lim}i}$ are never required when projecting the matrices. Hence, $k_{\Lambda,x,j}$ and $k_{\Theta,y,j}$ are not needed.

The unknown values can be obtained using experimental data to optimize the model so that the values of the unknowns yield the smallest error between the measured and the predicted values of stiffness of the whole robot.

Consider $N$ experiments in which the robot is in configurations defined by ${}^{O}\mathbf{r}_{T,n}$ and ${}^{O}\hat{\mathbf{t}}_n$, $n = 1, \ldots, N$. In each experiment, a force $F_n$ is applied at $T$ in the direction $\hat{\mathbf{u}}_n$, and the displacement $\delta_{\Lambda,\hat{\mathbf{u}}_n,\text{exp}n}$ of $T$ in the same direction is measured.

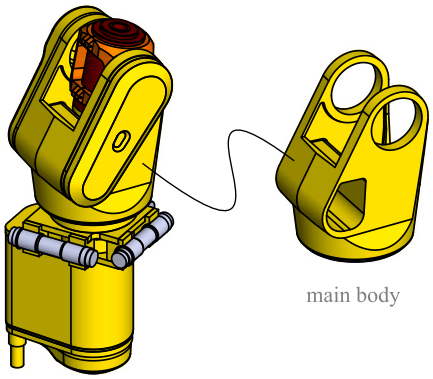


**Fig. 7.** Components in the serial module.

Since the inverse kinematics is known, given the configuration of the robot in each experiment, a predicted value of such displacement can be computed in terms of $\mathbf{v}$ after obtaining the displacement vector ${}^{\mathrm{T}}\Delta\mathbf{X}$ in frame T. Thus, the corresponding prediction is given by $\delta_{\Lambda,\hat{\mathbf{u}}_n,\mathrm{pred}n}({}^{\mathrm{O}}\mathbf{r}_{T,n}, {}^{\mathrm{O}}\hat{\mathbf{t}}_n)(\mathbf{v}) := {}^{\mathrm{T}}\Delta\mathbf{X}({}^{\mathrm{O}}\mathbf{r}_{T,n}, {}^{\mathrm{O}}\hat{\mathbf{t}}_n)(\mathbf{v}) \cdot (\mathbf{O}; \hat{\mathbf{u}}_n)$. It follows that for every experiment we wish to minimize the error:

$$\epsilon_n(\mathbf{v}) := \left(\delta_{\Lambda,\hat{\mathbf{u}}_n,\mathrm{pred}n}({}^{\mathrm{O}}\mathbf{r}_{T,n}, {}^{\mathrm{O}}\hat{\mathbf{t}}_n)(\mathbf{v}) - \delta_{\Lambda,\hat{\mathbf{u}}_n,\mathrm{exp}n}\right)^2, \; n = 1, \ldots, N \tag{26}$$

The problem thus becomes a multiobjective optimization (MOO) in which the observed trend can be imposed by adding constraints into our problem. For example, consider experiments 1, 2 and 3 were carried out along direction $\hat{\mathbf{u}}$ and show a trend such that $\delta_{\Lambda,\hat{\mathbf{u}}_1,\mathrm{exp}1} < \delta_{\Lambda,\hat{\mathbf{u}}_2,\mathrm{exp}2} < \delta_{\Lambda,\hat{\mathbf{u}}_3,\mathrm{exp}3}$, then the minimization problem in hand would be stated as:

- Minimize:

$$\epsilon_n(\mathbf{v}) := \left(\delta_{\Lambda,\hat{\mathbf{u}}_n,\mathrm{pred}n}({}^{\mathrm{O}}\mathbf{r}_{T,n}, {}^{\mathrm{O}}\hat{\mathbf{t}}_n)(\mathbf{v}) - \delta_{\Lambda,\hat{\mathbf{u}}_n,\mathrm{exp}n}\right)^2, \; n = 1, 2, 3$$

- Subject to:

$$\delta_{\Lambda,\hat{\mathbf{u}},\mathrm{pred}1}({}^{\mathrm{O}}\mathbf{r}_{T,1}, {}^{\mathrm{O}}\hat{\mathbf{t}}_1)(\mathbf{v}) - \delta_{\Lambda,\hat{\mathbf{u}},\mathrm{pred}2}({}^{\mathrm{O}}\mathbf{r}_{T,2}, {}^{\mathrm{O}}\hat{\mathbf{t}}_2)(\mathbf{v}) < 0$$
$$\delta_{\Lambda,\hat{\mathbf{u}},\mathrm{pred}2}({}^{\mathrm{O}}\mathbf{r}_{T,2}, {}^{\mathrm{O}}\hat{\mathbf{t}}_2)(\mathbf{v}) - \delta_{\Lambda,\hat{\mathbf{u}},\mathrm{pred}3}({}^{\mathrm{O}}\mathbf{r}_{T,3}, {}^{\mathrm{O}}\hat{\mathbf{t}}_3)(\mathbf{v}) < 0$$
$$\mathbf{v} \in V$$

where $V$ is the search space.

Since this is a MOO problem, we are searching for a Pareto frontier rather than a single optimum. The Pareto frontier is the set of individuals (or solutions) in which it is not possible to find a single solution that has a better fitness than the solutions in the set with respect to all the objective functions. Hence, such a change will worsen at least one objective.

Different algorithms can be used to find this Pareto frontier, including the skyline query method [35], the scalarization algorithm [36], simulated annealing [37], genetic algorithms and direct multisearch (DMS) [31]. These last two are available in the Global Optimization Toolbox from Matlab©. Both genetic algorithms and DMS are derivative-free algorithms, which is important for the problem in hand since the objective functions are so complex that we will consider them as black boxes that take a candidate $\mathbf{v}$ and return $\epsilon_i$.

In this paper we use the `paretosearch` function in the Global Optimization Toolbox from Matlab© which executes the DMS algorithm to find the Pareto frontier. DMS is a pattern search algorithm, which means it uses a search/poll method extending the poll in the directions where constraints-satisfactory non-dominated solutions were found. The algorithm stops when the hypervolume delimited by the frontier changed less than a tolerance. For a detailed explanation and proof of convergence see Custódio et al. [31] and the algorithm Matlab page.

Fig. 8 shows the flow diagram of the steps followed to determine optimal values of the unknown variables $\mathbf{v}_{\mathrm{opt}}$

## 9. Case study

Experiments were carried out on the Exechon XMini with offset wrist shown in Fig. 9a. Table 3 shows the dimensions of the manipulator. The experiments setup is shown in Fig. 9b

The stiffness is calculated by dividing the known magnitude of a force being applied at the tool tip over its corresponding displacement. A known force is applied by rotating a screw while using a force sensor to measure the real-time force value. The applied force is derived and recorded from the acquisition system of the piezoelectric sensor. For measuring the displacement,

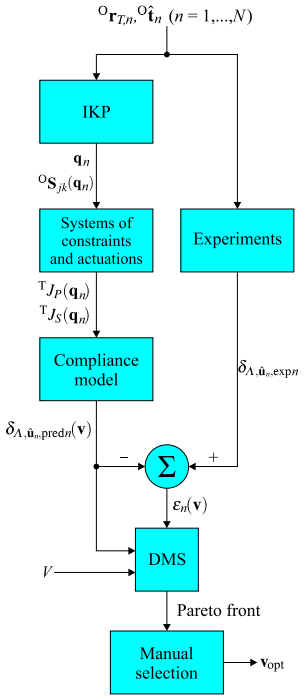


**Fig. 8.** Method followed to determine $\mathbf{v}_{opt}$.

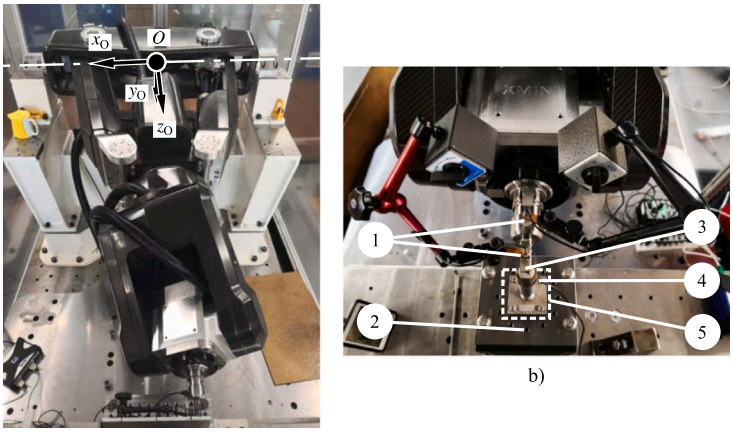


a) b)

**Fig. 9.** (a) The Exechon XMini used for the experiments and its fixed coordinate system O. (b) Experiments setup: 1. Eddy current sensor, 2. Fixture of loading system, 3. Tool tip, 4. Force sensor, 5. Loading system (force along $y_O$).

**Table 3**
Dimensions of the Exechon XMini in mm.

| Name | Value | Name | Value | Name | Value |
|---|---|---|---|---|---|
| $h_y$ | 33 | $h_z$ | 520 | $d_S$ | 50 |
| $d_{A1}$ | 250 | $d_{A2}$ | 400 | $d_{B1}$ | 133 |
| $d_{B2}$ | 166 | $d_T$ | 210 | | |

high-accuracy eddy current sensing system is employed. The eddy current sensor head was fixed right behind or closely beside the target area to measure the displacement under a known force. We employed high accurate eddy current sensor and calibrated them within an accuracy of 2 μm. That means, these sensor could measure the deformation at micro level. The data is then captured and processed.

**Table 4**
Experiments used for the optimization process ($F_n = -100$ N and ${}^{O}\hat{\mathbf{t}}_n = {}^{O}\hat{\mathbf{u}}_n = {}^{O}\hat{\mathbf{k}}$, $n = 1, \dots, 4$)

| $n$ | ${}^{O}\mathbf{r}_{T,n}$ (mm) | $\delta_{\Lambda,\hat{\mathbf{u}}_n,\mathrm{exp}n}$ (mm) |
|---|---|---|
| 1 | (0, 260, 1355) | −0.8350047575e−2 |
| 2 | (−138, 260, 1355) | −0.9881549403e−2 |
| 3 | (−340, 260, 1355) | −0.1171779778e−1 |
| 4 | (−408, 260, 1355) | −0.1413836810e−1 |

FEM was applied to the elements gimbal, gimbal1, gimbal2 and axisg2. The following compliance constants were obtained in the directions of their corresponding fixed frame (all quantities in mm/N):

$$\begin{aligned}
\mathbf{C}_{\Theta,\mathrm{gim}} &= \mathrm{diag}(\times, \times, 4.170527354 \times 10^{-15}) \\
\mathbf{C}_{\Lambda,\mathrm{gim}} &= \mathrm{diag}(9.52 \times 10^{-7}, 1.6 \times 10^{-5}, 2 \times 10^{-6}) \\
\mathbf{C}_{\Lambda,\mathrm{gim1}} &= \mathrm{diag}(6.95 \times 10^{-6}, 7.098 \times 10^{-6}, 1.47 \times 10^{-6}) \\
\mathbf{C}_{\Lambda,\mathrm{gim2}} &= \mathrm{diag}(3.324 \times 10^{-7}, 1.839 \times 10^{-9}, 7.852 \times 10^{-7}) \\
\mathbf{C}_{\Lambda,\mathrm{axisg2}} &= \mathrm{diag}(2.887 \times 10^{-6}, 7.434 \times 10^{-7}, 1.426 \times 10^{-7})
\end{aligned}$$

For the main body of the serial module the following values were obtained using FEM:

$$\begin{aligned}
c_{cS1}^{cS1} &= 4.269 \times 10^{-8} \text{ mm/N} \\
c_{cS2}^{cS2} &= 0.94 \times 10^{-4} \text{ mm/N} \\
c_{cS3}^{cS3} &= 5 \times 10^{-7} \text{ mm/N} \\
c_{cS4}^{cS4} &= 2.109281437 \times 10^{-15} \text{ Nmm}
\end{aligned}$$

However, due to the complexity of the mounting of the main body and the way it is connected to legs 1 and 3, the compliance of the large gimbal (element gim) was included in the optimization process as a variable. This also ensures that the effect of the compliance of the bearings supporting legs 1 and 3 through the large gimbal is considered in the result. Similarly, the compliance of the main body in the serial module was included in the optimization process, due to its interaction with the spindle, its mounting, and the different components included in the serial module.

Hence, $\mathbf{v}$ consists of variables $k_{\Lambda,y,1}$, $k_{\Lambda,y,2}$, $k_{\Lambda,z,1}$, $k_{\Lambda,z,2}$, $k_{\Theta,x,1}$, $k_{\Theta,x,2}$, $k_{\Theta,z,1}$, $k_{\Theta,z,2}$, $c_{\mathrm{act}}$, $c_{aS1}^{aS1}$, $c_{aS2}^{aS2}$, $c_{cS1}^{cS1}$, $c_{cS2}^{cS2}$, $c_{cS3}^{cS3}$, $c_{cS4}^{cS4}$, $c_{\Lambda,x,\mathrm{gim}}$, $c_{\Lambda,y,\mathrm{gim}}$, $c_{\Lambda,z,\mathrm{gim}}$, and $c_{\Theta,z,\mathrm{gim}}$, where $\mathrm{diag}(c_{\Lambda,x,\mathrm{gim}}, c_{\Lambda,y,\mathrm{gim}}, c_{\Lambda,z,\mathrm{gim}}) = \mathbf{C}_{\Lambda,\mathrm{gim}}$.

Firstly, four experiments are carried out and are used in the MOO. The results of these experiments are shown in Table 4. The results show the corresponding linear displacement along $\hat{\mathbf{u}}$, due to a force of magnitude $F$ and direction $\hat{\mathbf{t}}$

In order to ease the computational cost of the optimization, the process is carried out in different stages. First, the FEM results of the gimbal and the main body of the serial module are used in order to not consider them as optimization variables. Only experiments 1, 2 and 4 are considered to enhance the time of conversion and to use the remaining experiment as a validation case. Hence, the first stage consists of:

- Variables:

$$\mathbf{v} := \left(k_{\Lambda,y,1}, k_{\Lambda,y,2}, k_{\Lambda,z,1}, k_{\Lambda,z,2}, k_{\Theta,x,1}, k_{\Theta,x,2}, k_{\Theta,z,1}, k_{\Theta,z,2}, c_{\mathrm{act}}, c_{aS1}^{aS1}, c_{aS2}^{aS2}\right)$$

- Minimize:

$$\epsilon_1(\mathbf{V}), \epsilon_3(\mathbf{V}), \epsilon_4(\mathbf{V})$$

- Subject to:

$$\begin{aligned}
&|\delta_{\Lambda,\hat{\mathbf{u}}_1,\mathrm{pred1}}| - |\delta_{\Lambda,\hat{\mathbf{u}}_3,\mathrm{pred3}}| < 0 \\
&|\delta_{\Lambda,\hat{\mathbf{u}}_3,\mathrm{pred3}}| - |\delta_{\Lambda,\hat{\mathbf{u}}_4,\mathrm{pred4}}| < 0 \\
&0 < v_j < 1 \times 10^{-4}
\end{aligned}$$

where $v_j$ are all the components of $\mathbf{v}$. Subsequently, the obtained values for the optimization variables are replaced and now the remaining variables of the original problem become the only optimization variables. Hence, the second stage is given by:

- Variables:

$$\mathbf{v} := \left(c_{cS1}^{cS1}, c_{cS2}^{cS2}, c_{cS3}^{cS3}, c_{cS4}^{cS4}, c_{\Lambda,x,\mathrm{gim}}, c_{\Lambda,y,\mathrm{gim}}, c_{\Lambda,z,\mathrm{gim}}, c_{\Theta,z,\mathrm{gim}}\right)$$

- Minimize:

$$\epsilon_1(\mathbf{V}), \epsilon_3(\mathbf{V}), \epsilon_4(\mathbf{V})$$

- Subject to:

$$|\delta_{\Lambda,\hat{\mathbf{u}}_1,\text{pred1}}| - |\delta_{\Lambda,\hat{\mathbf{u}}_3,\text{pred3}}| < 0$$
$$|\delta_{\Lambda,\hat{\mathbf{u}}_3,\text{pred3}}| - |\delta_{\Lambda,\hat{\mathbf{u}}_4,\text{pred4}}| < 0$$
$$0 < v_j < 1 \times 10^{-4}$$

Finally, the variables modeling the leg element are optimized again, now considering experiment 2 instead of 3. This allows adjusting the results to a better fit to all four points. As such, experiment 4 will be used for validation. However, stage 1 suggested that all $k_{\Lambda,y,2}$, $k_{\Lambda,z,2}$, $k_{\Theta,x,2}$ and $k_{\Theta,z,2}$ should be zero. Therefore, we do not consider these variables in the third optimization, which is stated as follows:

- Variables:

$$\mathbf{v} := \left(k_{\Lambda,y,1}, k_{\Lambda,z,1}, k_{\Theta,x,1}, k_{\Theta,z,1}, c_{\text{act}}\right)$$

- Minimize:

$$\epsilon_1(\mathbf{V}), \epsilon_2(\mathbf{V}), \epsilon_4(\mathbf{V})$$

- Subject to:

$$|\delta_{\Lambda,\hat{\mathbf{u}}_1,\text{pred1}}| - |\delta_{\Lambda,\hat{\mathbf{u}}_2,\text{pred2}}| < 0$$
$$|\delta_{\Lambda,\hat{\mathbf{u}}_2,\text{pred2}}| - |\delta_{\Lambda,\hat{\mathbf{u}}_4,\text{pred4}}| < 0$$
$$0 < v_j < 1 \times 10^{-4}$$

The resulting optimized values of the whole process are the following:

$$k_{\Lambda,y,1} = 9.375 \times 10^{-6}\text{N}^{-1} \qquad k_{\Lambda,y,2} = 0$$
$$k_{\Lambda,z,1} = 6.77626 \times 10^{-21}\text{N}^{-1} \qquad k_{\Lambda,z,2} = 0$$
$$k_{\Theta,x,1} = 5 \times 10^{-6}\text{N}^{-1} \qquad k_{\Theta,x,2} = 0$$
$$k_{\Theta,z,1} = 5 \times 10^{-6}\text{N}^{-1} \qquad k_{\Theta,z,2} = 0$$
$$c_{\text{act}} = 4.8688 \times 10^{-5}\ \text{mm/N}$$
$$c^{aS1}_{aS1} = 1 \times 10^{-4}\ \text{rad/Nmm}$$
$$c^{aS2}_{aS2} = 1.3552 \times 10^{-20}\ \text{rad/Nmm}$$
$$c^{cS1}_{cS1} = 3.3854 \times 10^{-5}\ \text{mm/N}$$
$$c^{cS2}_{cS2} = 6.7762 \times 10^{-21}\ \text{mm/N}$$
$$c^{cS3}_{cS3} = 5.2083 \times 10^{-6}\ \text{mm/N}$$
$$c^{cS4}_{cS4} = 6.09375 \times 10^{-5}\ \text{rad/Nmm}$$
$$c_{\Lambda,x,\text{gim}} = 1 \times 10^{-10}\ \text{mm/N}$$
$$c_{\Lambda,y,\text{gim}} = 7 \times 10^{-7}\ \text{mm/N}$$
$$c_{\Lambda,z,\text{gim}} = 1 \times 10^{-9}\ \text{mm/N}$$
$$c_{\Theta,z,\text{gim}} = 5 \times 10^{-7}\ \text{rad/Nmm}$$

Additional six experiments were carried out in order to validate the optimized compliance model. The definition and results of these experiments are shown in Table 5. Table 5 also shows the deformation values predicted by our optimized model and the corresponding error against the experimental values. Each optimization was carried out on a commercial laptop with 16 Gb in RAM and a processor speed of 2.90 GHz, the most longest running time detected in an optimization was 1:58 min. From Table 5, it can be seen that results in the $z_{\text{O}}$-direction are satisfactory, with a maximum error of 10.354%. The maximum error in the $x_{\text{O}}$-direction is 19.998%. The largest error were found in the $y_{\text{O}}$-direction with a maximum of 39.206%. Fig. 10 shows the map for linear stiffness in the $z_{\text{O}}$ along working planes parallel to the $x_{\text{O}}z_{\text{O}}$ plane with different values of the coordinate $y_{\text{O}}$.

**A word on gravity:** Following the method presented in [13], it is not too difficult to include the effect of gravity in the model presented in this paper. However, since we are trying to fit our model to the results of experiments on the actual machine, the effect of gravity is not required at least at the stage of optimizing the unknown constants of the model. The total deflection of the manipulator at its end-effector contains two components: a deflection due to gravity and a deflection due to the external force applied at the end-effector. The deflection due to gravity (acting along the $y_{\text{O}}$-direction in our experiments) is permanent and independent of the external load. Say the controller is ordered to position the tip of the end-effector at ${}^{\text{O}}\mathbf{r}_T$. Due to gravity, the robot will present a deflection before starting the experiment, and the real position of the tip will be ${}^{\text{O}}\mathbf{r}_{T,\text{grav}}$. Once the external force is applied the position of the tool will change to ${}^{\text{O}}\mathbf{r}_{T,\text{F}}$. However, in our experiments, it is only feasible to measure the difference between ${}^{\text{O}}\mathbf{r}_{T,\text{F}}$ and ${}^{\text{O}}\mathbf{r}_{T,\text{grav}}$, since it is not possible to measure ${}^{\text{O}}\mathbf{r}_{T,\text{grav}}$ with the precision required for any analysis. Since the displacement measured in the experiments is that produced by the external force alone, the gravity effect should not be considered in order to learn the unknown parameters. Nevertheless, our IKP should be solved for ${}^{\text{O}}\mathbf{r}_{T,\text{grav}}$, which we do not. Therefore, we give a 1-mm compensation due to gravity, namely, we solve the IKP for ${}^{\text{O}}\mathbf{r}_T - (0,1,0)$

**Table 5**
Experiments carried out on the Exechon XMini and comparison to predicted values. For all $n = 1, \ldots, 10$, the displacement corresponds to $F_n = -100$ N and ${}^{O}\hat{\mathbf{t}}_n = {}^{O}\hat{\mathbf{k}}$.

| $n$ | ${}^{O}\mathbf{r}_{T,n}$ (mm) | $\hat{\mathbf{u}}_n$ | $\delta_{\Lambda,\hat{\mathbf{u}}_n,\mathrm{exp}n}$ (mm) | $\delta_{\Lambda,\hat{\mathbf{u}}_n,\mathrm{pred}n}$ (mm) | Error (%) |
|---|---|---|---|---|---|
| 1 | (0,260,1355) | (0,0,1) | −0.008350048 | −0.008836983611 | 5.831536068 |
| 2 | (−138,260,1355) | (0,0,1) | −0.009881549 | −0.008858429 | 10.353846730 |
| 3 | (−340,260,1355) | (0,0,1) | −0.011717798 | −0.011669665 | 0.410765409 |
| 4 | (−408,260,1355) | (0,0,1) | −0.014138368 | −0.014477298 | 2.397235293 |
| 5 | (−68,260,1355) | (0,0,1) | −0.0081281849 | −0.008617324 | 6.017820104 |
| 6 | (−276,260,1355) | (0,0,1) | −0.010702398 | −0.010174949 | 4.928314859 |
| 7 | (85,260,1450) | (1,0,0) | −0.090090090 | −0.092380377 | 2.542218887 |
| 8 | (323,260,1450) | (1,0,0) | −0.086206897 | −0.103380147 | 19.920970321 |
| 9 | (0,225,1450) | (0,1,0) | −0.082644628 | −0.115046523 | 39.206293228 |
| 10 | (408,226,1450) | (0,1,0) | −0.105263158 | −0.124294783 | 18.080043731 |

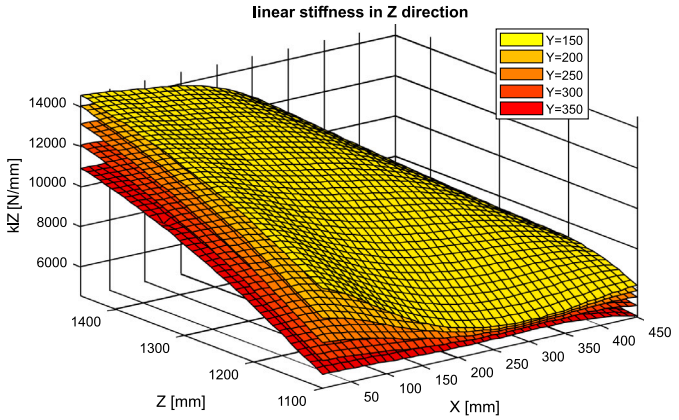


**Fig. 10.** Maps of linear stiffness in the $Z_O$-direction along the working plane $X_O Z_O$.

## 10. Conclusions

This paper presented the inverse kinematics and a compliance model for Exechon manipulators with offset wrists. The inverse kinematics was solved also considering offsets between the axes of the joints connecting the limbs to the base. The IKP was reduced to two systems of 4 non-linear equations in 4 unknowns. It was shown that when the offsets at the base are equal to zero, a single univariable polynomial can be obtained. In practice, however, we prefer to use the two systems of 4 non-linear equations even if the offsets at the base do not exist. The reason being that by solving numerically these two systems, two solutions are secured. This allows more control in the selection of solutions when automating the process.

The compliance model was obtained by proposing a general model for the local compliance of elements that encompass multiple mechanical components of the robot. The local compliance values of these elements were modeled as a 2-degree polynomial in the leg length. The unknowns of the model were then optimized using experimental data. Subsequently, more experiments were carried out to validate the model. The resulting model was able to predict the compliance along the $z_O$-direction with a maximum error of around 10%. In the $x_O$-direction the worst error was measured as 19%. However, the prediction in the $y_O$-direction gave a maximum error of 39.2%.

## Declaration of competing interest

The authors declare that they have no known competing financial interests or personal relationships that could have appeared to influence the work reported in this paper.

## Acknowledgments

This work was supported by the Engineering and Physical Sciences Research Council (EPSRC), UK projects with reference numbers EP/P025447/1 and EP/P026087/1. The support from Northern Ireland Technology Centre for the experimental work is also acknowledged.

## References


[1] J. Merlet, Parallel Robots, Springer Netherlands, Heidelberg, Germany, 2006.
[2] X. Kong, C. Gosselin, Type Synthesis of Parallel Mechanisms, Springer-Verlag Berlin Heidelberg, 2007.
[3] D. Stewart, A platform with six degrees of freedom, Proc. Inst. Mech. Eng. 180 (1) (1965) 371–386.
[4] B. Dasgupta, T. Mruthyunjaya, The Stewart platform manipulator: a review, Mech. Mach. Theory 35 (1) (2000) 15–40.
[5] K.-E. Neumann, Robot, US Patent US4732525A, 1985.
[6] B. Siciliano, The Tricept robot: Inverse kinematics, manipulability analysis and closed-loop direct kinematics algorithm, Robotica 17 (4) (1999) 437–445.
[7] K.-E. Neumann, The key to aerospace automation, in: SAE Technical Paper, SAE International, 2006.
[8] K.-E. Neumann, Parallel-kinematical machine, US Patent US20090205457A1, 2014.
[9] M. Shang, J. Butterfield, The experimental test and FEA of a PKM (Exechon) in a flexible fixture application for aircraft wing assembly, in: 2011 IEEE International Conference on Mechatronics and Automation, 2011, pp. 1225–1230.
[10] J. Zhang, Y. Zhao, Y. Jin, Kinetostatic-model-based stiffness analysis of Exechon PKM, Robot. Comput.-Integr. Manuf. 37 (2016) 208–220.
[11] J. Zhang, Y. Zhao, Y. Jin, Elastodynamic modeling and analysis for an exechon parallel kinematic machine, J. Manuf. Sci. Eng. 138 (2015) 138–141.
[12] X. Li, D. Zlatanov, M. Zoppi, R. Molfino, Stiffness estimation and experiments for the exechon parallel self-reconfiguring fixture mechanism, in: International Design Engineering Technical Conferences and Computers and Information in Engineering Conference, Chicago, IL, Canada, 2012, pp. 637–645.
[13] M. Wang, H. Liu, T. Huang, D.G. Chetwynd, Compliance analysis of a 3-SPR parallel mechanism with consideration of gravity, Mech. Mach. Theory 84 (2015) 99–112.
[14] Z. Bi, Y. Jin, Kinematic modeling of exechon parallel kinematic machine, Robot. Comput.-Integr. Manuf. 27 (1) (2011) 186–193.
[15] Y. Jin, Z. Bi, H. Liu, C. Higgings, M. Price, W. Chen, T. Huang, Kinematic analysis and dimensional synthesis of exechon parallel kinematic machine for large volume machining, J. Mech. Robot. 7 (4) (2015).
[16] M. Zoppi, D. Zlatanov, R. Molfino, 2010,
[17] P. López-Custodio, J. Dai, R. Fu, Y. Jin, Kinematics and constraints of the exechon robot accounting offsets due to errors in the base joint axes, J. Mech. Robot. 12 (2) (2020) 021109.
[18] M. Raghavan, B. Roth, Inverse kinematics of the general 6R manipulator and related linkages, J. Mech. Des. 115 (3) (1993) 502–508.
[19] Y. Wang, H. Liu, T. Huang, D.G. Chetwynd, Stiffness modeling of the tricept robot using the overall Jacobian matrix, J. Mech. Robot. 1 (2) (2009) 021002.
[20] Z. Wei, B. Li, Y. Hu, Stiffness analysis of a hybrid manipulator applied to a multi-dimensional vibration isolator, in: IEEE International Conference on Mechatronics and Automation, Chengdu, China, 2012, pp. 1874–1879.
[21] C. Gosselin, Stiffness mapping for parallel manipulators, IEEE Trans. Robot. Autom. 6 (3) (1990) 377–382.
[22] S.A. Joshi, L.-W. Tsai, JacobiAn analysis of limited-DOF parallel manipulators, J. Mech. Des. 124 (2) (2002) 254–258.
[23] Y. Li, E. Zhang, Y. Song, Z. Feng, Stiffness modeling and analysis of a novel 4-DOF PKM for manufacturing large components, Chin. J. Aeronaut. 26 (6) (2013) 1577–1585.
[24] Y. Li, Q. Xu, Stiffness analysis for a 3-PUU parallel kinematic machine, Mech. Mach. Theory 43 (2) (2008) 186–200.
[25] A.G. Hoevenaars, P. Lambert, J.L. Herder, Jacobian-based stiffness analysis method for parallel manipulators with non-redundant legs, Proc. Inst. Mech. Eng. C 230 (3) (2016) 341–352.
[26] A. Pashkevich, D. Chablat, P. Wenger, Stiffness analysis of overconstrained parallel manipulators, Mech. Mach. Theory 44 (5) (2009) 966–982.
[27] X. Ding, J. Dai, Compliance analysis of mechanisms with spatial continuous compliance in the context of screw theory and Lie groups, Proc. Inst. Mech. Eng. C 224 (11) (2010) 2493–2504.
[28] S. Wang, G. Cheng, Y. Pang, G. Lodewijks, Integrated stiffness analysis of redundant parallel manipulator based on finite element method, J. Inf. Comput. Sci. 121 (2015) 351–365.
[29] D. Deblaise, X. Hernot, P. Maurine, A systematic analytical method for PKM stiffness matrix calculation, in: Proceedings 2006 IEEE International Conference on Robotics and Automation, 2006, ICRA 2006, 2006, pp. 4213–4219.
[30] G. Carbone, M. Ceccarelli, A stiffness analysis for a hybrid parallel-serial manipulator, Robotica 22 (5) (2004) 567–576.
[31] A.L. Custódio, J.F.A. Madeira, A.I.F. Vaz, L.N. Vicente, Direct multisearch for multiobjective optimization, SIAM J. Optim. 21 (3) (2011) 1109–1140.
[32] C. Crane, J. Duffy, Kinematic Analysis of Robot Manipulators, Cambridge University Press, Cambridge, 1998.
[33] F. Xi, D. Zhang, C.M. Mechefske, S.Y. Lang, Global kinetostatic modelling of tripod-based parallel kinematic machine, Mech. Mach. Theory 39 (4) (2004) 357–377.
[34] T. Pigoski, M. Griffis, J. Duffy, Stiffness mappings employing different frames of reference, Mech. Mach. Theory 33 (6) (1998) 825–838.
[35] F. Nielsen, Output-sensitive peeling of convex and maximal layers, Inform. Process. Lett. 59 (5) (1996) 255–259.
[36] I.Y. Kim, O.L. de Weck, Adaptive weighted sum method for multiobjective optimization: a new method for Pareto front generation, Struct. Multidiscip. Optim. 31 (2) (2006) 105–116.
[37] A. Suppapitnarm, K.A. Seffen, G.T. Parks, P.J. Clarkson, A simulated annealing algorithm for multiobjective optimization, Eng. Optim. 33 (1) (2000) 59–85.